

การเปรียบเทียบปริมาณรังสียังผลในหุ่นจำลองจากการตรวจเอกซเรย์คอมพิวเตอร์  
โดยวิธีมอนติคาร์โลกับการวัดจากเครื่องวัดรังสีแบบเทอร์โมลูมิเนสเซนส์



นายบุญเสริม เนยสูงเนิน

## สถาบันวิทยบริการ จุฬาลงกรณ์มหาวิทยาลัย

วิทยานิพนธ์นี้เป็นส่วนหนึ่งของการศึกษาตามหลักสูตรปริญญาวิทยาศาสตรมหาบัณฑิต

สาขาวิชาฉายเวชศาสตร์ ภาควิชารังสีวิทยา

คณะแพทยศาสตร์ จุฬาลงกรณ์มหาวิทยาลัย

ปีการศึกษา 2550

ลิขสิทธิ์ของจุฬาลงกรณ์มหาวิทยาลัย

**COMPARISON OF EFFECTIVE DOSE IN PHANTOM FROM  
COMPUTED TOMOGRAPHY USING MONTE CARLO  
SIMULATION AND THERMOLUMINESCENT  
DOSIMETRY METHODS**



**Mr.Boonserm Nerysungnoen**


สถาบันวิทยบริการ  
จุฬาลงกรณ์มหาวิทยาลัย

**A Thesis Submitted in Partial Fulfillment of the Requirements  
for the Degree of Master of Science Program in Medical Imaging  
Department of Radiology  
Faculty of Medicine  
Chulalongkorn University  
Academic Year 2007  
Copyright of Chulalongkorn University**

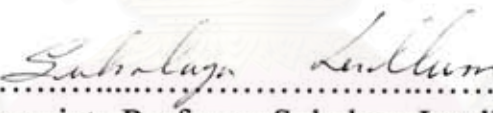
Thesis Title                    COMPARISON OF EFFECTIVE DOSE IN  
  PHANTOM                    FROM                    COMPUTED  
  TOMOGRAPHY USING MONTE CARLO  
  SIMULATION AND THERMOLUMINESCENT  
  DOSIMETRY METHODS  
By                                    Mr.Boonserm Nerysungnoen  
Field of Study                    Medical Imaging  
Thesis Advisor                   Associate Professor Sivalee Suriyapee, M.Eng.


---

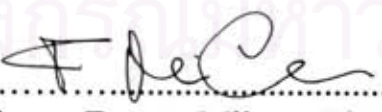
Accepted by the Faculty of Medicine, Chulalongkorn University in  
Partial Fulfillment of the Requirements for the Master's Degree

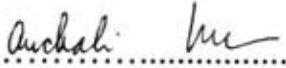
  
.....Dean of the Faculty of Medicine  
(Associate Professor Adisorn Patradul, M.D.)

THESIS COMMITTEE:

  
.....Chairman  
(Associate Professor Sukalaya Lerdlum, M.D., M.Sc.)

  
.....Thesis Advisor  
(Associate Professor Sivalee Suriyapee, M.Eng.)

  
.....External Member  
(Professor Franco Milano, Ph.D.)

  
.....Member  
(Associate Professor Anchali Krisanachinda, Ph.D.)

บุญเสริม เนษสูงเนิน : การเปรียบเทียบปริมาณรังสียังผลในหุ่นจำลองจากการตรวจเอกซเรย์คอมพิวเตอร์โดยวิธีมอนติคาร์โลกับการวัดจากเครื่องวัดรังสีแบบเทอร์โมลูมิเนสเซนซ์ (COMPARISON OF EFFECTIVE DOSE IN PHANTOM FROM COMPUTED TOMOGRAPHY USING MONTE CARLO SIMULATION AND THERMOLUMINESCENT DOSIMETRY METHODS) อ.ที่ปรึกษา: รศ.ศิวลี สุรียาปี; 80 หน้า

การตรวจด้วยเครื่องเอกซเรย์คอมพิวเตอร์ทางด้านรังสีวินิจฉัยเป็นการตรวจที่มีความจำเป็นเพื่อวินิจฉัยโรคที่เกิดขึ้นแต่ในขณะเดียวกันนั้นการตรวจแต่ละครั้งพบว่าผู้ป่วยจะได้รับปริมาณรังสีที่สูง การวิจัยครั้งนี้ศึกษาวิธีการคำนวณหาปริมาณรังสีดูดกลืนและรังสียังผลแบบใช้โปรแกรมอิมแพคท์สเฟรคซิทคำนวณโดยวิธีมอนติคาร์โลและการวัดในหุ่นจำลองโดยใช้เครื่องวัดรังสีแบบเทอร์โมลูมิเนสเซนซ์

การคำนวณและการวัดปริมาณรังสีดูดกลืนและรังสียังผลได้ทำจากการตรวจเอกซเรย์คอมพิวเตอร์ช่องอกและช่องท้องจากเครื่องเอกซเรย์คอมพิวเตอร์ซีเมนต์เซนเซชัน 16 ที่โรงพยาบาลจุฬาลงกรณ์สภากาชาดไทย การคำนวณจะทำการวัดหาค่าซีทีดีไอ ที่อากาศและในหุ่นจำลองด้วยเครื่องวัด สแกนดิทรมอนิคซ์/เวลล์สอพเฟอร์ รุ่นซีที 10 - อาร์เอส ไอออนไนซ์เซนชันแชมเบอร์ หลังจากนั้นนำค่าที่วัดได้และค่าพารามิเตอร์ที่ใช้ในการตรวจไปใส่ลงในโปรแกรมเพื่อคำนวณปริมาณรังสีดูดกลืนและรังสียังผลที่อวัยวะต่างๆออกมา การวัดใช้เครื่องวัดรังสีแบบเทอร์โมลูมิเนสเซนซ์เทียบเคียงมาตรฐานกับรังสีโคบอลต์-60 โดยศึกษาเพื่อหาความไว ความสัมพันธ์เชิงเส้น และการตอบสนองของเครื่องวัดรังสีแบบเทอร์โมลูมิเนสเซนซ์แล้วทำการใส่เครื่องวัดรังสีในหุ่นจำลองแล้วนำหุ่นจำลองไปตรวจเอกซเรย์คอมพิวเตอร์ช่องอกและช่องท้อง แล้วทำการคำนวณปริมาณรังสีดูดกลืนและรังสียังผล ในขั้นสุดท้ายนำผลทั้งสองวิธีมาหาค่าเปอร์เซ็นต์ความแตกต่าง

จากการศึกษาของเราในครั้งนี้ปริมาณรังสีดูดกลืนจากการตรวจทั้งเอกซเรย์คอมพิวเตอร์ช่องอกและช่องท้องพบว่าวิธีการวัดในหุ่นจำลองโดยใช้เครื่องวัดรังสีแบบเทอร์โมลูมิเนสเซนซ์จะมีค่าสูงกว่าการคำนวณโดยวิธีมอนติคาร์โล ยกเว้นในตำแหน่ง หลอดอาหาร และพื้นผิวของกระดูกสำหรับการตรวจเอกซเรย์คอมพิวเตอร์ในช่องอก และในอวัยวะเพศ ปอด และหลอดอาหารสำหรับการตรวจเอกซเรย์คอมพิวเตอร์ช่องท้อง เมื่อพิจารณาอวัยวะที่อยู่ภายในลำรังสี ยกเว้นอวัยวะที่หาจุดวางตำแหน่งในการวัดได้ยาก ความแตกต่างของปริมาณรังสีดูดกลืนทั้งสองวิธีอยู่ใน 11.74 เปอร์เซ็นต์ ซึ่งเป็นค่าความไม่แน่นอนของเครื่องวัดรังสีแบบเทอร์โมลูมิเนสเซนซ์ ปริมาณรังสียังผลในการตรวจเอกซเรย์คอมพิวเตอร์ช่องอกโดยวิธีมอนติคาร์โลมีค่าเท่ากับ 4.37 มิลลิซีเวิร์ต และโดยวิธีวัดในหุ่นจำลองด้วยเครื่องวัดรังสีแบบเทอร์โมลูมิเนสเซนซ์มีค่าเท่ากับ 5.42 มิลลิซีเวิร์ต ความแตกต่างอยู่ใน 19.37 เปอร์เซ็นต์ ปริมาณรังสียังผลในการตรวจเอกซเรย์คอมพิวเตอร์ช่องท้องโดยวิธีมอนติคาร์โลมีค่าเท่ากับ 7.31 มิลลิซีเวิร์ต และโดยวิธีวัดในหุ่นจำลองด้วยเครื่องวัดรังสีแบบเทอร์โมลูมิเนสเซนซ์มีค่าเท่ากับ 8.52 มิลลิซีเวิร์ต ความแตกต่างอยู่ใน 14.20 เปอร์เซ็นต์ ผลที่ได้ปริมาณจากการวัดในหุ่นจำลองจะสูงกว่าการคำนวณโดยวิธีมอนติคาร์โลซึ่งก็สอดคล้องกับงานวิจัยของคนอื่น สาเหตุเนื่องมาจากการออกแบบหุ่นจำลองที่แตกต่างกันระหว่างแรนโดแฟมทอมที่ใช้ในการวัดกับแมทเธแมททิกคอลแฟมทอมที่ใช้ในการจำลองในวิธีมอนติคาร์โล ดังนั้นการประเมินค่าปริมาณรังสีที่ผู้ป่วยได้รับ สามารถใช้วิธีคำนวณแบบมอนติคาร์โลได้แต่ต้องทราบว่าค่าที่ได้จะต่ำกว่าค่าจริงภายใน 20 เปอร์เซ็นต์

ภาควิชา.....รังสีวิทยา.....ลายมือชื่อนิสิต *Janak Anur*  
 สาขาวิชา.....ฉายาเวชศาสตร์.....ลายมือชื่ออาจารย์ที่ปรึกษา *อ.อ.ส. สุรียาปี*  
 ปีการศึกษา.....2550.....

# # 4974737030: MAJOR MEDICAL IMAGING

KEYWORD: EFFECTIVE DOSE / COMPUTED TOMOGRAPHY / MONTE CARLO SIMULATION / THERMOLUMINESCENT DOSIMETRY.

BOONSERM NERYSUNGNOEN: COMPARISON OF EFFECTIVE DOSE IN PHANTOM FROM COMPUTED TOMOGRAPHY USING MONTE CARLO SIMULATION AND THERMOLUMINESCENT DOSIMETRY METHODS. THESIS ADVISOR: ASSOC. PROF. SIVALEE SURIYAPEE, 80 pp.

Computed tomography (CT) is the examination procedure in diagnostic radiology and the dose given to the patient is higher than general radiographic procedures. This research work is to study the organ doses and effective doses from calculation by ImPACT spreadsheet of Monte Carlo simulation and measurement by thermoluminescent dosimeter (TLD) in the Rando phantom.

The organ doses and effective doses for chest and abdominal examinations were estimated from Siemens Sensation 16 computed tomography equipment used at King Chulalongkorn Memorial Hospital. The computed tomography dose index (CTDI) was measured in air and in body phantom with Scanditronix/Wellhofer DCT 10-RS ionization chamber then the CTDIs and exposed parameters were entered in ImPACT spreadsheet for calculation of the organ and effective doses. The TLD-100 chips were calibrated with  $^{60}\text{Co}$  beams. The sensitivity, linearity and energy response of TLD-100 chips were determined. The TLD-100 chips were inserted in the Rando phantom and were irradiated. The organ doses and effective doses were calculated. Finally, the results from two methods were compared in term of percentage difference.

From our study, most of the organ doses for chest and abdominal examinations from thermoluminescent dosimetry were higher than those calculated by Monte Carlo simulation except breast, esophagus, and bone surfaces for chest examination and gonads, lung, and esophagus for abdominal examination. The differences between the organ doses from two methods were within the 11.74% uncertainty of TLD measurement for the organ located in the radiation field except the organs that were difficult to search for the exact location. The effective doses of chest examination were 4.37 mSv from Monte Carlo simulation and 5.42 mSv for thermoluminescent dosimetry, resulted in 19.37% difference. The effective doses of abdominal examination were 7.31 mSv from Monte Carlo simulation and 8.52 mSv for thermoluminescent dosimetry, resulted in 14.20% difference. The results showed the higher measured dose than calculated which agreed with the other published studies. The underestimation of the calculated dose was mainly due to the difference of the design between the Rando phantom and Medical Internal Radiation Dosimetry (MIRD) mathematical phantom in Monte Carlo simulation. For the clinical patient, the organ and effective doses could be estimated by Monte Carlo simulation with the awareness of the under estimation within 20%.

Department ..... Radiology ..... Student's signature *B. Nerysungnoen*  
 Field of study ..... Medical Imaging ..... Advisor's signature *Sivalee Suriyapee*  
 Academic year ..... 2007 .....

## ACKNOWLEDGEMENTS

The success of this thesis could be attributed to the extensive support and assistance from my major advisor, Assoc. Prof. Sivalee Suriyapee and my co-advisor, Mr.Sornjarod Oonsiri. I deeply thank them for their valuable advice and guidance in this research.

I wish to thank my thesis committee, Assoc. Prof. Sukalaya Lerdlum, Diagnostic Division, Department of Radiology, Assoc. Prof. Anchali Krisanachinda, Nuclear Medicine Division, Faculty of Medicine, Chulalongkorn University and Professor Franco Milano, Florence University, Italy, for their kindness, helpful and valuable suggestion.

I would like to thank Assoc. Prof. Somjai Wangsuphachart, Chief of Department of Radiology, Faculty of Medicine, Chulalongkorn University for her kindness, helpful and valuable suggestion.

I would like to thank Mrs.Weeranuch Kitsukjit for her provide suggestion for the improvement, Mr.Walop Makmool helped for experiment in the research and Mr.Nuntawat Ou-dee introduced for MATLAB.

I would like to thank Ms.Chotika Jampangern, Mr.Taweap Sanghangthum, Mr.Isra Israngkul Na Ayuthaya, Ms.Pantiwa Insang and medical staff in Division of Radiation Oncology, Department of Radiology, King Chulalongkorn Memorial Hospital for their kindness in examining the research instrument and providing suggestions for improvement.

I would like to thank medical staffs in the computed tomography room, Department of Radiology, King Chulalongkorn Memorial Hospital for their kindness in examining the research instrument and providing suggestions for improvement.

I am grateful to all the lecturers and staff of Medical Imaging, Chulalongkorn University, for supplying me academic knowledge on Medical Imaging.

Finally, I am grateful to my family for their financial support, entirely care, and love. The usefulness of this thesis, I dedicate to my father, my mother and all the teachers.

จุฬาลงกรณ์มหาวิทยาลัย

# CONTENTS

	<b>Page</b>
ABSTRACT (THAI).....	iv
ABSTRACT (ENGLISH).....	v
ACKNOWLEDGEMENTS.....	vi
CONTENTS.....	vii
LIST OF TABLES.....	ix
LIST OF FIGURES.....	x
LIST OF ABBREVIATIONS.....	xiii
<b>CHAPTER 1 INTRODUCTION.....</b>	<b>1</b>
1.1 Background and rationale.....	1
1.2 Research objective.....	1
<b>CHAPTER 2 REVIEW OF RELATED LITERATURES.....</b>	<b>2</b>
2.1 Theory.....	2
2.1.1 Computed tomography .....	2
2.1.2 Radiation dose in computed tomography .....	9
2.1.3 Thermoluminescent dosimetry .....	13
2.1.4 Estimating effective dose from computed tomography... ..	20
2.1.5 ImPACT dose survey.....	21
2.1.6 The ImPACT program.....	24
2.2 Literature review.....	28
<b>CHAPTER 3 RESEARCH METHODOLOGY.....</b>	<b>30</b>
3.1 Research design.....	30
3.2 Research design model.....	30
3.3 Conceptual framework.....	30
3.4 Keywords.....	31
3.5 Research question.....	31
3.6 Materials.....	31
3.6.1 The pencil ionization chamber.....	31
3.6.2 The electrometer.....	32
3.6.3 Monte Carlo simulation program.....	32
3.6.4 The body phantom.....	33
3.6.5 The computed tomography equipment.....	33
3.6.6 The Alderson Rando phantom.....	34
3.6.7 The thermoluminescent dosimeters.....	34
3.6.8 The automatic thermoluminescent dosimeter reader... ..	35
3.6.9 The cobalt-60 teletherapy machine.....	35
3.6.10 Water phantom.....	36
3.7 Methods.....	36
3.7.1 Monte Carlo simulation method.....	36
3.7.2 Thermoluminescent dosimetry method.....	41
3.8 Data collection.....	44
3.9 Data analysis.....	44

	<b>Page</b>
3.9.1	Uncertainty of TLD measurement..... 44
3.9.2	Summarization of data..... 45
3.9.3	Data presentation..... 45
3.10	Benefit of the study..... 45
3.11	Ethic consideration..... 45
<b>CHAPTER 4</b>	<b>RESULTS..... 46</b>
4.1	Monte Carlo simulation..... 46
4.1.1	Measurement of computed tomography dose index..... 46
4.1.2	The organ doses and effective doses from Monte Carlo simulation..... 46
4.2	Thermoluminescent dosimetry..... 48
4.2.1	Thermoluminescent dosimeter characteristics..... 48
4.2.2	Uncertainty of TLD measurement..... 53
4.2.3	The organ doses and effective doses from thermoluminescent dosimetry..... 54
4.3	Comparison the organ doses and effective doses between two methods..... 56
4.3.1	Chest examination..... 56
4.3.2	Abdominal examination..... 58
<b>CHAPTER 5</b>	<b>DISCUSSION AND CONCLUSION..... 60</b>
5.1	Discussion..... 60
5.1.1	The comparison of computed tomography dose index from measured, calculated, and ImPACT values..... 60
5.1.2	The uncertainty of thermoluminescent dosimeters..... 60
5.1.3	Comparison of the organ and effective doses between Monte Carlo simulation and thermoluminescent dosimetry..... 60
5.2	Conclusion..... 62
<b>REFERENCES</b>	<b>..... 64</b>
<b>APPENDICES</b>	<b>..... 66</b>
Appendix A:	Case record forms..... 67
Appendix B:	Report of computed tomography system performance..... 69
Appendix C:	Uncertainty of TLD measurement..... 78
<b>VITAE</b>	<b>..... 80</b>



## LIST OF TABLES

<b>Table</b>	<b>Page</b>
3.1 Computed tomography exposure factors and protocols.....	43
4.1 Computed tomography dose index in the air and the body phantom.....	46
4.2 The organ doses, tissue doses and effective doses of chest examination by Monte Carlo simulation.....	47
4.3 The organ doses, tissue doses and effective doses of abdominal examination by Monte Carlo simulation.....	48
4.4 The sensitivity correction values of 67 thermoluminescent dosimeter chips that were used for measurement.....	49
4.5 The sensitivity correction values of 11 thermoluminescent dosimeter chips that were used for calibration.....	49
4.6 The absorbed doses in $^{60}\text{Co}$ and reading value of thermoluminescent dosimeter responses.....	50
4.7 Reading values of thermoluminescent dosimeters for radiation profile.....	51
4.8 Reading values of background.....	52
4.9 Uncertainty budgets and the expanded uncertainty of dose measurement using TLD measurement in Rando phantom.....	53
4.10 The organ doses, tissue doses and effective doses of thermoluminescent dosimetry for chest examination.....	54
4.11 The organ doses, tissue doses and effective doses of thermoluminescent dosimetry for abdominal examination.....	55
4.12 Comparison of the organ doses and effective doses between thermoluminescent dosimetry and Monte Carlo simulation for chest examination.....	56
4.1 Comparison of the organ doses and effective doses between thermoluminescent dosimetry and Monte Carlo simulation for abdominal examination.....	58
5.1 Comparison of effective doses with the other studies for chest examination.....	61
5.2 Comparison of effective doses with the other studies for abdominal examination.....	62

## LIST OF FIGURES

<b>Figure</b>	<b>Page</b>
2.1 Postero-anterior and lateral chest radiographs.....	3
2.2 Pixel and voxel of a digital image.....	3
2.3 Two types of computed tomography beam projection.....	4
2.4 Data acquisition in computed tomography.....	5
2.5 Schematic diagram apparatus for thermoluminescence dose measurement.....	13
2.6 A simplified energy-level diagram of thermoluminescence process.....	14
2.7 The glow curve of lithium fluoride.....	15
2.8 An example of thermoluminescence versus absorbed dose curve for TLD-100 powder.....	16
2.9 Relation of half value layer to effective energy.....	17
2.10 Theoretical sensitivity of thermoluminescence phosphors.....	18
2.11 Mathematical phantom.....	21
2.12 The dose distribution of a computed tomography scanner.....	22
2.13 Correlation of x-ray beam half-value layer and normalized effective dose for abdominal examinations.....	23
2.14 Correlation of ImPACT factor and normalized effective dose for abdominal examinations.....	24
2.15 The ImPACT program.....	25
3.1 Research design model.....	30
3.2 Conceptual framework.....	30
3.3 The pencil ionization chamber.....	31
3.4 The electrometer.....	32
3.5 The ImPACT spreadsheet.....	32

<b>Figure</b>	<b>Page</b>
3.6 The body phantom.....	33
3.7 The computed tomography equipment.....	33
3.8 The Alderson Rando phantom.....	34
3.9 The thermoluminescent dosimeters and plastic tubes.....	34
3.10 The automatic thermoluminescent dosimeter reader.....	35
3.11 The cobalt-60 teletherapy machine.....	35
3.12 Water phantom.....	36
3.13 The pencil chamber at the isocenter in air.....	37
3.14 The pencil chamber at the center of the body phantom.....	37
3.15 The pencil chamber at the peripheries of the body phantom.....	37
3.16 The ImPACT spreadsheet program.....	38
3.17 The procedure of calculation.....	39
3.18 Start and end positions of scan range.....	40
3.19 The report of calculation.....	40
3.20 The phantom with thermoluminescent dosimeters for radiation profile measurement.....	42
3.21 The marked position of some organs in a single slice of the phantom.....	43
3.22 The Rando phantom scanning.....	43
3.23 The unit of the automatic thermoluminescent dosimeter reader.....	44
4.1 The relation between thermoluminescent dosimeters and absorbed doses response.....	50
4.2 Manual plotted of radiation profile of 10 mm slice thickness.....	51
4.3 MATLAB plotted of radiation profile of 10 mm slice thickness.....	52

<b>Figure</b>	<b>Page</b>
4.4 The correlation of the organ doses from thermoluminescent dosimetry with 11.74% uncertainty of TLD measurement and Monte Carlo simulation of chest examination.....	57
4.5 The correlation of the effective doses from thermoluminescent dosimetry with 11.74% uncertainty of TLD measurement and Monte Carlo simulation of abdominal examination.....	59



สถาบันวิทยบริการ  
จุฬาลงกรณ์มหาวิทยาลัย

## LIST OF ABBREVIATIONS

<b>Abbreviation</b>	<b>Terms</b>
2D	Two dimension
3D	Three dimension
A	Atomic mass
Al <sub>2</sub> O <sub>3</sub>	Aluminum oxide
BG	Background
°c	Degree celcius
CaCO <sub>3</sub>	Calcium carbonate
CaF <sub>2</sub>	Calcium fluoride
CaSO <sub>4</sub>	Calcium sulfate
cGy	centigray
cm	centimeter
cm <sup>3</sup>	Cubic centimeter
<sup>60</sup> Co	Cobalt-60
<sup>137</sup> Cs	Cesium-137
CT	Computed tomography
CTDI	Computed tomography dose index
CV	Coefficient of variation
DLP	Dose-length product
ECC	Element correction coefficient
FOV	Field of view
g/cm <sup>3</sup>	gram per cubic centimeter
ICRP	International Commission on Radiological Protection

<b>Abbreviation</b>	<b>Terms</b>
ICRU	International Commission on Radiation Units and Measurement
ImPACT	Imaging Performance Assessment of computed tomography
keV	kiloelectronvolt
kV	kilovoltage
kVp	kilovolt-peak
Li <sub>2</sub> B <sub>4</sub> O <sub>7</sub>	Lithium borate
LiF	Lithium fluoride
mAs	milliamper-second
MDD	Minimum detectable dose
MeV	Megaelectronvolt
Mg	Magnesium
mGy	milligray
MIRD	Medical Internal Radiation Dosimetry
mJ	millijoule
mm	millimeter
mmAl	millimeter-aluminum
MSAD	Multiple scan average dose
MSCT	Multi-slice computed tomography
mSv	millisievert
nC	nanocoulomb
NRPB	National Radiological Protection Board
PA	Postero-anterior

<b>Abbreviation</b>	<b>Terms</b>
PMMA	Polymethyl methacrylate
PMT	Photomultiplier tube
QC	Quality control
R	Roentgen
rad/R	Radiation absorbed dose per Roentgen
RCF	Reader calibration factor
SD	Standard deviation
SiO <sub>2</sub>	Silicon oxide
Sv	Sievert
Ti	Titanium
TLD	Thermoluminescent dosimeter
Z	Atomic number
$\mu_a/\rho_a$	Mass energy absorption coefficient of air
$\mu_t/\rho_t$	Mass energy absorption coefficient of the tissue

สถาบันวิทยบริการ  
จุฬาลงกรณ์มหาวิทยาลัย

# CHAPTER 1

## INTRODUCTION

### 1.1 Background and rationale

The Computed tomography (CT) was introduced into clinical practice in the early 1970s and revolutionized x-ray imaging by providing high quality images which reproduced transverse cross sections of the body. Tissues are therefore not superimposed on the image as they are in conventional projections. The technique offered in particular improved low contrast resolution for better visualization of soft tissue, but with relatively high absorbed radiation dose. The National Radiological Protection Board (NRPB) has developed a coherent method for estimating absorbed dose to the organs of patients undergoing CT examinations. Full details of the methods and results of the survey are given in a series of three NRPB reports [1 - 3].

In Thailand the CT is the significant source of diagnostic x-ray exposure for Thai population. The increasing used of CT made more than 200 CT machines over the country. Approximate of over million Thai people were CT scanner per year. This will increase the collective dose in Thailand.

An individual CT patient dose is not possible to be measured for the exact effective dose. Dose estimation is made by using computed tomography dose index (CTDI) measurements and normalized doses obtained from data tables produced by Monte Carlo simulations. These tables are published by NRPB and were employed in the national survey of CT practice in the United Kingdom [3]. The tables were derived from simulations of the Medical Internal Radiation Dosimetry (MIRD) mathematical phantom [4], for a variety of CT machines. The Monte Carlo method is convenient but it is dependent on the CT unit design. For these reasons we decided to measure the organ doses and effective doses from the 16 detector multi-slice for chest and abdominal examinations, directly using thermoluminescent dosimeters (TLDs) and Rando phantom, and compared with the Monte Carlo simulation.

The purpose of this study determined the organ doses and effective doses by Monte Carlo simulation and TLD measurement. Finally, the results were compared.

### 1.2 Research objective

To compare the effective doses between calculated by Monte Carlo simulation and thermoluminescent dosimetry.



## CHAPTER 2

### REVIEW OF RELATED LITERATURES

#### 2.1 Theory

##### 2.1.1 Computed tomography

##### 2.1.1.1 Basic principle [5]

The mathematical principles of CT were first developed by Radon in 1917. Radon's treatise proved that an image of an unknown object could be produced if one had an infinite number of projections through the object. We can understand the basic idea behind tomographic imaging with an example taken from radiography.

With plain film imaging, the three-dimensional (3D) anatomy of the patient is reduced to a two-dimensional (2D) projection image. The density at a given point on an image represents the x-ray attenuation properties within the patient along a line between the x-ray focal spot and the point on the detector corresponding to the point on the image. Consequently, with a conventional radiograph of the patient's anatomy, information with respect to the dimension parallel to the x-ray beam is lost. This limitation can be overcome, at least for obvious structures, by acquiring both a postero-anterior (PA) projection and a lateral projection of the patient. For example, the PA chest image yields information concerning height and width, integrated along the depth of the patient, and the lateral projection provides information about the height and depth of the patient, integrated over the width dimension, they are shown in figure 2.1. For objects that can be identified in both images, such as a pulmonary nodule on PA and lateral chest radiographs, the two films provide valuable location information. For more complex or subtle pathology, however, the two projections are not sufficient. Imagine the instead of just two projections, a series of 360 radiographs were acquired at 1-degree angular intervals around the patient's thoracic cavity. Such a set of images provides essentially the same data as a thoracic CT scan. However, the 360 radiographic images display the anatomic information in a way that would be impossible for a human to visualize: cross-sectional images. If these 360 images were stored into a computer, the computer could in principle reformat the data and generate a complete thoracic CT examination.

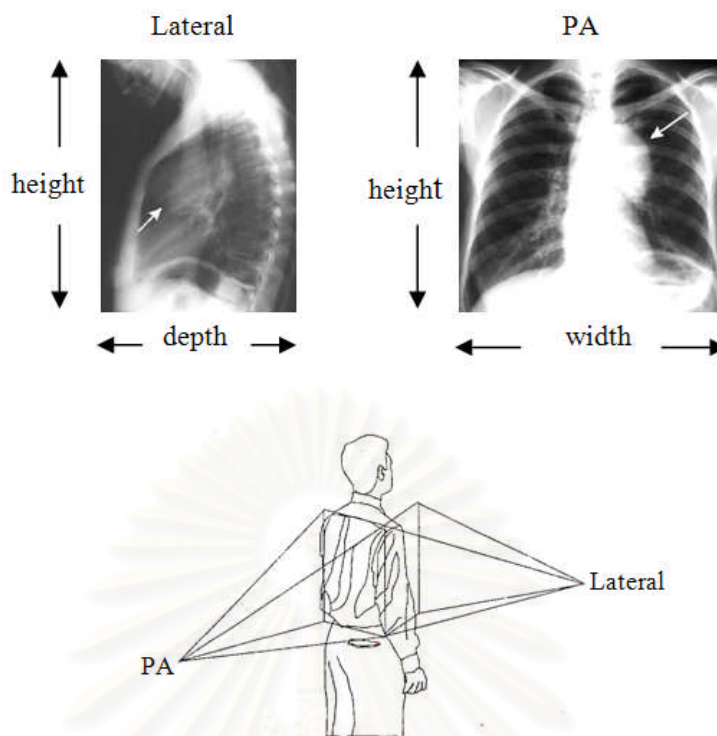


**Figure 2.1** Postero-anterior and lateral chest radiographs.

The tomographic image is a picture of a slice of the patient's anatomy. The 2D CT image corresponds to a 3D section of the patient, so that even with CT, three dimensions are compressed into two. However, unlike the case with plain film imaging, the CT slice-thickness is very thin (1 to 10 mm) and is approximately uniform. The 2D array of pixels (picture elements) in the CT image corresponds to an equal number of 3D voxels (volume elements) in the patient. Voxels have the same in-plane dimensions as pixels, but they also include the slice thickness dimension. Each pixel on the CT image displays the average x-ray attenuation properties of the tissue in the corresponding voxel, it is shown in figure 2.2.

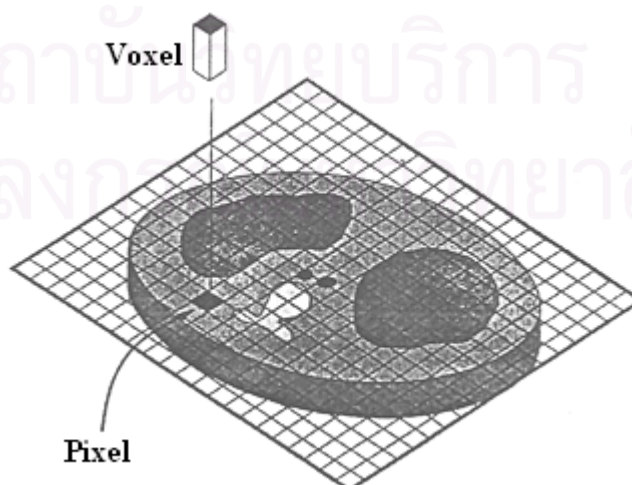


**Figure 2.2** Pixel and voxel of a digital image.

### 2.1.1.2 Tomographic acquisition [5]

A single transmission measurement through the patient made by a single detector at a given moment in time is called a ray. A series of rays that pass through the patient at the same orientation is called a projection or view. There are two projection geometries that have been used in CT imaging, they are shown in figure 2.3. The more basic type is parallel beam geometry, in which all of the rays in a projection are parallel to each other. In fan beam geometry, the rays at a given projection angle diverge and have the appearance of a fan. All modern CT scanners incorporate fan beam geometry in the acquisition and reconstruction process. The purpose of the CT scanner hardware is to acquire a large number of transmission measurements through the patient at different positions. The acquisition of a single axial CT image may involve approximately 800 rays taken at 1,000 different projection angles, for a total of approximately 800,000 transmission measurements. Before the axial acquisition of the next slice, the table that the patient is lying on is moved slightly in the cranial-caudal direction (the z-axis of the scan), which positions a different slice of tissue in the path of the x-ray beam for the acquisition of the next image.

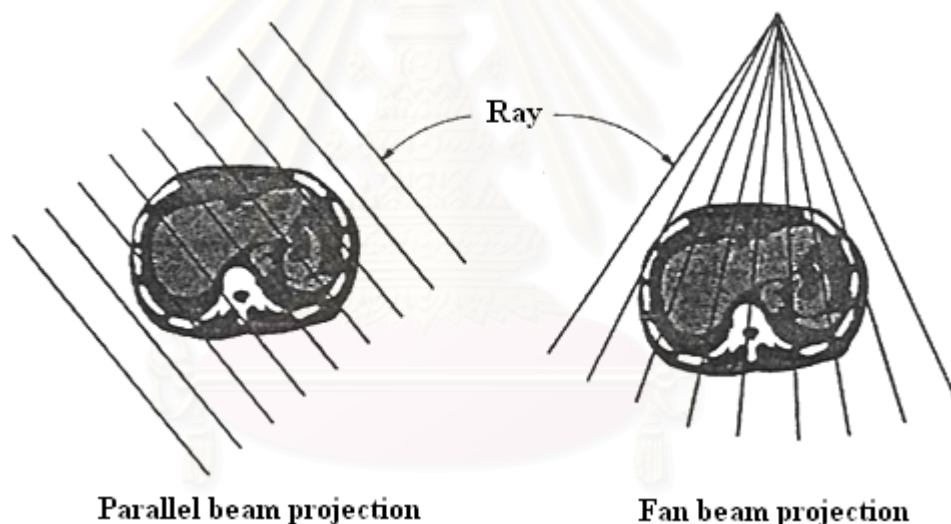


**Figure 2.3** Two types of computed tomography beam projection.

### 2.1.1.3 Tomographic reconstruction [5]

Each ray that is acquired in CT is a transmission measurement through the patient along a line, where the detector measures an x-ray intensity,  $I_t$ . The unattenuated intensity of the x-ray beam is also measured during the scan by a reference detector, and this detects an x-ray intensity  $I_0$ . The relationship between  $I_t$  and  $I_0$  is given by

$$I_t = I_0 e^{-\mu t} \quad (2.1)$$

Where  $t$  is the thickness of the patient along the ray and  $\mu$  is the average linear attenuation coefficient along the ray. Notice that  $I_t$  and  $I_0$  are machine-dependent values, but the product  $\mu t$  is an important parameter relating to the anatomy of the patient along a given ray. When the equation is rearranged, the measured values  $I_t$  and  $I_0$  can be used to calculate the parameter of interest:

$$\ln\left(\frac{I_0}{I_t}\right) = \mu t \quad (2.2)$$

Where  $\ln$  is the natural logarithm (to base  $e$ ,  $e = 2.78\dots$ ),  $t$  ultimately cancels out, and the value  $\mu$  for each ray is used in the CT reconstruction algorithm. This computation, which is a preprocessing step performed before image reconstruction, reduces the dependency of the CT image on the machine-dependent parameters, resulting in an image that depends primarily on the patient's anatomic characteristics. This is very much a desirable aspect of imaging in general, and the high clinical utility of CT results, in part, from this feature. By comparison, if it is overexposed ( $I_0$  too high) it appears too dark. The density of CT images is independent of  $I_0$ , although the noise in the image is affected.

After preprocessing of the raw data, a CT reconstruction algorithm is used to produce the CT images. There are numerous reconstruction strategies; however, filtered back projection reconstruction is most widely used in clinical CT scanners. The back projection method builds up the CT image in the computer by essentially reversing the acquisition steps, it is shown in figure 2.4. During acquisition, attenuation information along a known path of the narrow x-ray beam is integrated by a detector. During back projection reconstruction, the  $\mu$  value for each ray is smeared along this same path in the image of the patient. As the data from a large number of rays are back projection onto the image matrix, areas of high attenuation tend to reinforce each other, and areas of low attenuation also reinforce, building up the image in the computer.

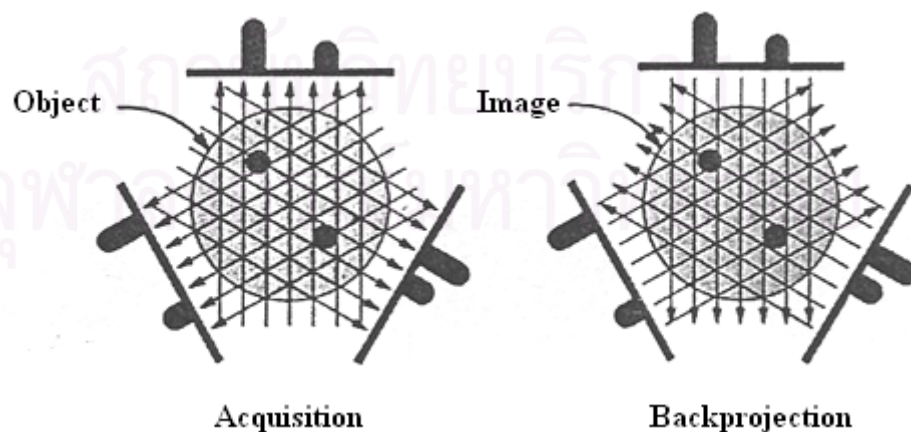


**Figure 2.4** Data acquisition in computed tomography.

### 2.1.1.4 Computed tomography number

After CT reconstruction, each pixel in the image is represented by a high-precision floating point number that is useful for computation but less useful for display. Most computer display hardware makes use of integer images. Consequently, after CT reconstruction, but before storing and displaying, CT images are normalized and truncated to integer values. The number  $CT(x,y)$  in each pixel,  $(x,y)$ , of the image is converted using the equation 2.3:

$$CT(x, y) = 1,000 \times \frac{\mu(x, y) - \mu_{water}}{\mu_{water}} \quad (2.3)$$

where  $\mu(x, y)$  is the floating point number of the  $(x, y)$  pixel before conversion,  $\mu_{water}$  is the attenuation coefficient of water, and  $CT(x, y)$  is the CT number (Hounsfield unit) that ends up in the final clinical CT image. The value of  $\mu_{water}$  is about 0.195 for the x-ray beam energies typically used in CT scanning. This normalization results in CT numbers ranging from about - 1,000 to + 3,000, where - 1,000 corresponds to air, soft tissues range from - 300 to - 100, water is 0, and dense bone and areas filled with contrast agent range up to + 3,000.

CT images are produced with a highly filtered, high-kV x-ray beam, with an average energy of about 75 keV. At this energy in muscle tissue, about 91% of x-ray interactions are Compton scatter. For fat and bone, Compton scattering interactions are 94% and 74%, respectively. Therefore, CT numbers and hence CT images derive their contrast mainly from the physical properties of tissue that influence Compton scatter. Density ( $\text{g/cm}^3$ ) is a very important discriminating property of tissue (especially in lung tissue, bone, and fat), and the linear attenuation coefficient,  $\mu$ , tracks linearly with density. Other than physical density, the Compton scatter cross section depends on the electron density ( $\rho_e$ ) in tissue:  $\rho_e = NZ/A$ , where N is Avogadro's number ( $6.023 \times 10^{23}$ , a constant), Z is the atomic number, and A is the atomic mass of the tissue. The main constituents of soft tissue are hydrogen (Z = 1, A = 1), carbon (Z = 6, A = 12), nitrogen (Z = 7, A = 14), and oxygen (Z = 8, A = 16). Carbon, nitrogen, and oxygen all have the same Z/A ratio of 0.5, so their electron densities are the same. Because the Z/A ratio for hydrogen is 1.0, the relative abundance of hydrogen in a tissue has some influence on CT number. Hydrogenous tissue such as fat is well visualized on CT. Nevertheless, density ( $\text{g/cm}^3$ ) plays the dominant role in forming contrast in medical CT.

CT numbers are quantitative, and this property leads to more accurate diagnosis in some clinical settings. For example, pulmonary nodules that are calcified are typically benign, and the amount of calcification can be determined from the CT image based on the mean CT number of the nodule. Measuring the CT number of a single pulmonary nodule is therefore common practice, and it is an important part of the diagnostic work-up. CT scanners measure bone density with good accuracy, and when phantoms are placed in the field along with the patient, quantitative CT techniques can be used to estimate bone density, which is useful in assessing fracture risk. CT is also quantitative in terms of linear dimensions, and therefore it can be used to accurately assess tumor volume or lesion diameter.

### 2.1.1.5 Geometry and historical development [5]

#### A) The first generation

CT scanners represent a marriage of diverse technologies, including computer hardware, motor control systems, x-ray detectors, sophisticated reconstruction algorithms, and x-ray tube/generator systems. The first generation of CT scanners employed a rotate/translate, pencil beam system. Only two x-ray detectors were used, and they measured the transmission of x-rays through the patient for two different slices. The acquisition of the numerous projections and the multiple rays per projection required that the single detector for each CT slice be physically moved throughout all the necessary positions. This system used parallel ray geometry. Starting at a particular angle, the x-ray tube and detector system translated linearly across the field of view (FOV), acquiring 160 parallel rays across a 24 cm FOV. When the x-ray tube/detector system completed its translation, the whole system was rotated slightly, and then another translation was used to acquire the 160 rays in the next projection. This procedure was repeated until 180 projections were acquired at 1 degree intervals.

#### B) The second generation

The next incremental improvement to the CT scanner was the incorporation of a linear array of 30 detectors. This increased the utilization of the x-ray beam by 30 times, compared with the detector used per slice in first-generation systems. A relatively narrow fan angle of 10 degree was used. In principle, a reduction in scan time of about 30-fold could be expected. However, this reduction time was not realized, because more data were acquired to improve image quality.

#### C) The third generation

The number of detectors used in the third-generation scanners was increased substantially (to more than 800 detectors), and the angle of the fan beam was increased so that the detector array formed an arc wide enough to allow the x-ray beam to interrogate the entire patient. Because detectors and the associated electronics arc expensive, this led to more expensive CT scanners. However, spanning the dimensions of the patient with an entire row of detectors eliminated the need for translation motion. The multiple detectors in the detector array capture the same number of ray measurements in one instant as was required by a complete translation in the earlier scanner systems. The mechanically joined x-ray tube and detector array rotation together around the patient without translation. The motion of third-generation CT is rotate/translate, referring to the rotation of the x-ray tube and the rotation of the detector array. By elimination of the translational motion, the scan time is reduced substantially.

#### D) The fourth generation

The fourth-generation CT scanners were designed to overcome the problem of ring artifacts. With the fourth-generation scanners, the detectors are removed from the rotating gantry and are placed in a stationary 360-degree ring around the patient, requiring many more detectors. Modern fourth-generation CT systems use about

4,800 individual detectors. Because the x-ray tube rotates and the detectors are stationary, fourth-generation CT is said to use a rotate/stationary geometry. During acquisition with a fourth-generation scanner, the divergent x-ray beam emerging from the x-ray tube forms a fan-shaped x-ray beam. However, the data are processed for fan beam reconstruction with each detector as the vertex of a fan, the rays acquired by each detector being fanned out to different positions of the x-ray source.

#### E) The fifth generation

A novel CT scanner has been developed specifically for cardiac tomographic imaging. This cine-CT scanner does not use a conventional x-ray tube; instead, a large arc of tungsten encircles the patient and lies directly opposite to the detector ring. The x-rays are produced from the focal track as a high-energy electron beam strikes the tungsten. There are no moving parts to this scanner gantry. The electron beam is produced in a cone-like structure (a vacuum enclosure) behind the gantry and is electronically steered around the patient so that it strikes the annular tungsten target. Cine-CT systems, also called electron beam scanners, are marketed primarily to cardiologists. They are capable of 50-msec scan times and can produce fast-frame-rate CT movies of the beating heart.

#### F) The sixth generation

In the early 1990s, the design of the third- and fourth-generation scanners evolved to incorporate slip ring technology. A slip ring is a circular contact with sliding brushes that allows the gantry to rotate continually, untethered by wires. The use of slip-ring technology eliminated the inertial limitations at the end of each slice acquisition, and the rotating gantry was free to rotate continuously throughout the entire patient examination. This design made it possible to achieve greater rotational velocities than with systems not using a slip ring, allowing shorter scan times. Helical CT (also inaccurately called spiral CT) scanners acquire data while the table is moving; as a result, the x-ray source moves in a helical pattern around the patient being scanned. Helical CT scanners use either third- and fourth-generation slip-ring designs. By avoiding the time required to translate the patient table, the total scan time required to image the patient can be much shorter. Consequently, helical scanning allows the use of less contrast agent and increase patient throughput. In some instances the entire scan can be performed within a single breath-hold of the patient, avoiding inconsistent levels of inspiration. The advent of helical scanning has introduced many different considerations for data acquisition. In order to produce reconstructions of planar sections of the patient, the raw data from the helical data set are interpolated to approximate the acquisition of planar reconstruction data. The speed of the table motion relative to the rotation of the CT gantry is a very important consideration, and the pitch is a parameter that describes this relationship.

#### G) The seventh generation

X-ray tubes designed for CT have impressive heat storage and cooling capabilities, although the instantaneous production of x-rays (i.e., x-rays per mAs) is constrained by the physics governing x-ray production. An approach to overcoming x-ray tube output limitations is to make better use of the x-rays that are produced by the x-ray tube. When multiple detector arrays were used, the collimator spacing was

wider and therefore more of the x-ray that was produced by the x-ray tube was used in producing image data. With conventional, single detector array scanners, opening up the collimator increases the slice thickness, which was good for improving the utilization of the x-ray beam but reduce spatial resolution in the slice thickness dimension. With the introduction of multiple detector arrays, the slice thickness was determined by the detector size and not by the collimator.

### 2.1.2 Radiation dose in computed tomography [6]

Because of its geometry and usage, CT is a unique modality and therefore has its own set of specific parameters for radiation dose. This modality is unique because the exposure is essentially continuous around the patient, rather than a projectional modality in which the exposure is taken from one or two source locations. The modality typically uses thin sections ranging from 0.5 mm to 20 mm nominal beam collimation. However, this modality also typically uses multiple exposures along some length of the patient to cover a volume of anatomy. In addition, these exposures may be done in sequences of scans (e.g., a series of scans such as pre- and post-contrast).

#### 2.1.2.1 Variations within the scan plane

Projectional radiographic exposures are taken from one source position and the entrance skin dose is much larger than the exit dose, creating a large radiation dose gradient across the patient. In contrast, the tomographic exposure of CT scans with a full 360° rotation results in a radially symmetric radiation dose gradient within patient. That is, in a uniform circular object, such as a test phantom, all of the points at a certain radius from the center have the same (or nearly the same) radiation dose. As we shall see, the magnitude of that dose gradient (the size of the difference from center to periphery) will be affected by several factors, including the size of the object, the x-ray beam spectrum, and the attenuation of the material or tissue.

For example, in a typical CT dosimetry phantom that is 32 cm in diameter and made of polymethyl methacrylate (PMMA) usually referred to as the body phantom measurements of CT dose, which will be defined later, obtained at the center are typically about 50% of the measured value obtained at one of the peripheral positions. This result which shows the center value obtained under specific conditions to be approximately 10 mGy while the peripheral values are 20 mGy under those same conditions. However, for a smaller-diameter phantom the 16 cm diameter phantom referred to as the head phantom measured under the identical exposure conditions, the center value reading climbs to approximately 40 mGy, as do the peripheral values. This indicates that the magnitude of the difference from center to periphery is very much size dependent; it also indicates that the absolute values of the absorbed doses are size dependent.

#### 2.1.2.2 Z-axis variations

In addition to variations within the scan plane, there are variations along the length of the patient or phantom. These can be characterized by the z-axis dose distribution or radiation profile. This is the distribution of absorbed dose along the axis of the patient due to a single axial scan (a full rotation at one table position). The radiation profile is not limited to the primary area being imaged, and there are tails to



this distribution from the nonideal collimation of the x-ray source and from scatter of photons within the object being exposed. When multiple adjacent scans are performed, the tails of the radiation profiles from adjacent scans can contribute to the absorbed dose outside of the primary area being imaged. If these tails are significant and are nonzero at some distance from the location of the originating section, then those contributions can add up, creating additional absorbed dose in the primary area being imaged.

That is the radiation dose in a specific section consist of the sum of contributions to that section when that area is the primary area being imaged as well as the contributions from the tails of radiation profiles from adjacent sections when other locations are the primary are being imaged. The size of the contributions from adjacent sections is very directly related to the spacing of sections and the width and shape of the radiation profile.

To account for the effects from multiple scans, several dose descriptors were developed. One of the first was the multiple scan average dose (MSAD) descriptors. This is defined as the average dose resulting from a series of scans over  $n$  interval ( $I$ ) in length:

$$MSAD = (1/I) \int_{-I/2}^{I/2} D_{series}(z) dz, \quad (2.4)$$

where  $I$  is the interval of the scan length and  $D_{series}(z)$  is the dose at position  $z$  parallel to the  $z$  (rotational) axis resulting from the series of CT scans.

Following this was the CTDI. This was defined as the radiation dose, normalized to beam width, measured from 14 contiguous sections:

$$CTDI = (1/nT) \int_{-7T}^{7T} D_{single}(z) dz, \quad (2.5)$$

where  $n$  is the number of sections per scan,  $T$  is the width of the interval equal to the selected section thickness, and  $D_{single}(z)$  is the dose at the point  $z$  on any line parallel to the  $z$  (rotational) axis for a single axial scan. This index was suggested by the Food and Drug Administration and incorporated into the code of federal regulation.

However, to be measured according to the definition, only 14 sections could be measured and one had to measure the radiation dose profile typically done with TLDs or film, neither of which was very convenient. Measurements of exposure could be obtained with a pencil ionization chamber, but its fixed length of 100 mm meant that 14 sections of 7 mm thickness could be measured with the chamber alone. To measure CTDI for thinner nominal sections, sometimes lead sleeves were used to cover the part of the chamber that exceeded 14 section widths.

To overcome the limitations of CTDI with 14 sections, another radiation dose index  $CTDI_{100}$  was developed. This index relaxed the constraint on 14 sections and allowed calculation of the index for 100 mm along the length of an entire pencil ionization chamber, regardless of the nominal section width being used. This index is therefore defined as

$$CTDI_{100} = (1/NT) \int_{-5cm}^{5cm} D_{single}(z) dz, \quad (2.6)$$

where  $N$  is the number of acquired sections per scan (also referred to as the number of data channels used during acquisition) and  $T$  is the nominal width of each acquired section (which is not necessarily the same as the nominal width of the reconstructed section width).

Because the ionization chamber measures an integrated exposure along its 100 mm length, this is equivalent to

$$CTDI_{100} = (f \cdot C \cdot E \cdot L)/(NT), \quad (2.7)$$

where  $f$  is the conversion factor from exposure to a dose in air (use 0.87 rad/R),  $C$  is the calibration factor for the electrometer,  $E$  is the measured value of exposure in roentgens acquired from a single  $360^\circ$  rotation with a beam profile of  $NT$  (as defined earlier),  $L$  is the active length of the pencil ionization chamber, and  $N$  and  $T$  are as defined for equation 2.6.

Thus, the exposure measurement, performed with one axial scan either in air or in one of the PMMA phantoms for which CTDI is defined, result in a calculated for the center location as well as at least one of the peripheral position (1 cm below the surface) within the phantom to describe the variations within the scan plane as well.

$CTDI_w$  was created to represent a dose index that provides a weighted average of the center and peripheral contributions to dose within the scan plane. The index is used to overcome the limitations of  $CTDI_{100}$  and its dependency on position within the scan plane. The definition is

$$CTDI_w = (1/3)(CTDI_{100})_{center} + (2/3)(CTDI_{100})_{periphery}, \quad (2.8)$$

One final CTDI descriptor takes into account the parameters that are related to a specific imaging protocol, the helical pitch or axial scan spacing, and is defined as  $CTDI_{vol}$ :

$$CTDI_{vol} = CTDI_w NT / I, \quad (2.9)$$

where  $N$  and  $T$  are as defined earlier and represent the total collimated width of the x-ray beam and  $I$  is the table travel per rotation for a helical scan or the spacing between acquisitions for axial scans.

For helical scans, the following formulas are used:

$$NT / I = 1 / pitch, \quad (2.10)$$

and

$$CTDI_{vol} = CTDI_w / pitch, \quad (2.11)$$

where *pitch* is defined as table distance traveled in one 360° rotation/total collimated width of the x-ray beam.

Another dose descriptor that is related to CTDI and is commonly reported on CT scanners and in the literature is the dose-length product (DLP) [7], this value is simply the  $CTDI_{vol}$  multiplied by the length of the scan (in centimeters) and is given in units of mGy.cm:

$$DLP = CTDI_{vol} \times Scanlength, \quad (2.12)$$

This descriptor is used in one approach to obtain an estimate of effective dose that will be described later.

These CTDI descriptors are obviously meant to serve as an index of radiation dose due to CT scanning and are not meant to serve as an accurate estimate of the radiation dose incurred by an individual patient. Although the phantom measurements are meant to be reflective of an attenuation environment somewhat similar to a patient, the homogeneous PMMA phantom does not simulate the different tissue types and heterogeneities of a real patient. In addition, the  $CTDI_{100}$  calculation uses the  $f$  factor (from equation 2.7) only to convert from exposure to a dose in air; other tissues have different  $f$  factors. The  $f$  factor (in units of rads per roentgen) is determined by the ratio of the mass energy absorption coefficient of a tissue to that of air:

$$f = 0.87 \times [(\mu_t / \rho_t) / (\mu_a / \rho_a)], \quad (2.13)$$

where  $\mu_t/\rho_t$  is the mass energy absorption coefficient of the tissue (e.g., bone, lung, soft tissue) and  $\mu_a/\rho_a$  is the mass energy absorption coefficient of air. The mass energy absorption coefficient depend not only the tissue but also on the energy of the photons, especially in the energy range used by CT. Thus, the  $CTDI_{100}$  calculation presents a very simplified condition for measuring radiation dose.

### 2.1.3 Thermoluminescent dosimetry [8]

In recent years many applications of TLD have been reported in the literature, and many more applications have gone unreported. There are hundreds of TLD readers in operation in various laboratories around the world. Many of dosimetry problems arising in radiation dosimetry can be resolved by using TLDs. The small size, good energy dependence, good sensitivity and large useful dose range of TLDs are key advantages, as the direct measurement of dose is possible under conditions in which other forms of dosimetry are not practical, measurement of the dose from the primary beam during fluoroscopy is convenient since the dosimeters do not interfere with the study [9]. There are several solid state systems available for the dosimetry of ionizing radiation. However, none of the systems provide absolute measurement—each needs calibration in a known radiation field before it can be used for the determination of absorbed dose. There are two types of solid state dosimeters: (a) integrating type dosimeters (thermoluminescent crystals, radiophotoluminescent glasses, optical density type dosimeters such as glass and film), and (b) electrical conductivity dosimeters (semiconductor junction detectors, induced conductivity in insulating materials). Of these, the most widely used systems for the measurement of absorbed dose are the TLDs, and film, which are described.

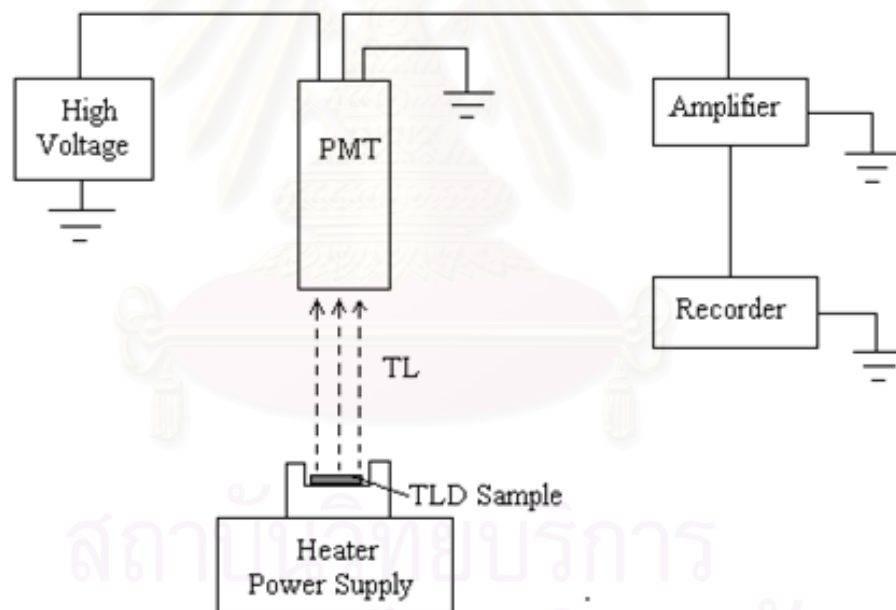


**Figure 2.5** Schematic diagram apparatus for thermoluminescence dose measurement.

Many crystalline materials exhibit the phenomenon of thermoluminescence used in TLDs. When such a crystal is irradiated, a very minute fraction of the absorbed energy is stored in the crystal lattice. Some of this energy can be recovered later as visible light if the material is heated. This phenomenon of release of visible photons by thermal means is known as thermoluminescence. The arrangement for measuring the thermoluminescence output is shown schematically in figure 2.5. The irradiated material is placed in a heater cup or planchet, where it is heated for a reproducible heating cycle. The emitted light is measured by a photomultiplier tube

(PMT) which converts light into an electrical current. The current is then amplified and measured by a recorder or a counter. There are several thermoluminescence phosphors available but the most noteworthy are lithium fluoride (LiF), lithium borate ( $\text{Li}_2\text{B}_4\text{O}_7$ ), and calcium fluoride ( $\text{CaF}_2$ ). Of these phosphors, LiF is most extensively studied and most frequently used for clinical dosimetry. LiF in its purest form exhibits relatively little thermoluminescence. But the presence of a trace amount of impurities (e.g., magnesium) provides the radiation-induced thermoluminescence. These impurities give rise to imperfections in the lattice structure of LiF and appear to be necessary for the appearance of the thermoluminescence phenomenon.

### 2.1.3.1 Simplified theory thermoluminescent dosimetry

The chemical and physical theory of the TLDs is not exactly known, but simple models have been proposed to explain the phenomenon qualitatively. Figure 2.6 shows an energy-level diagram of an inorganic crystal exhibiting thermoluminescence by ionizing radiation.

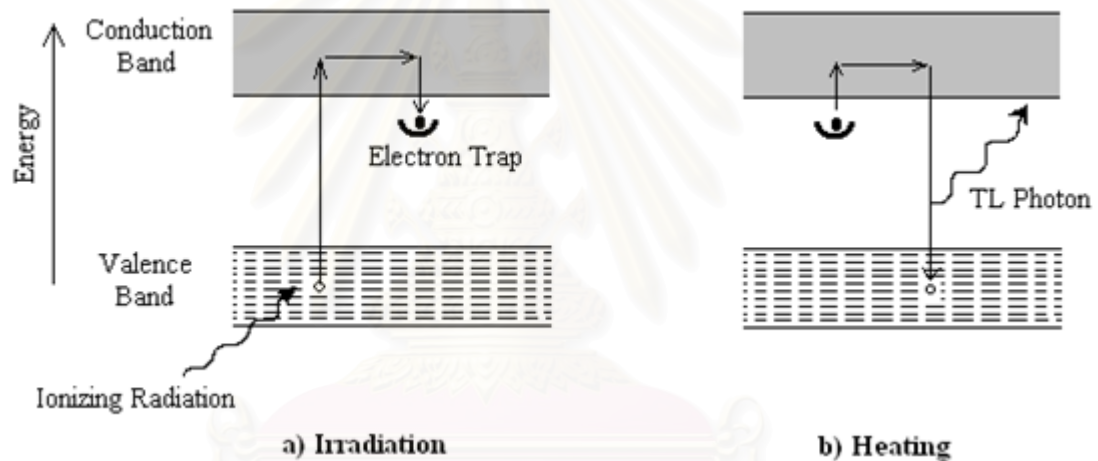


**Figure 2.6** A simplified energy-level diagram of thermoluminescence process.

In an individual atom, electron occupies discrete energy levels. In a crystal lattice, on the other hand, electronic energy levels are perturbed by mutual interactions between atoms and give rise to energy bands the “allowed” energy bands and forbidden energy bands. In addition, the presence of impurities in the crystal creates energy traps in the forbidden region, providing metastable states for the electrons. When the material is irradiated, some of the electrons in the valence band (ground state) receive sufficient energy to be raised to the conduction band. The vacancy thus created in the valence band is called a positive hole. The electron and the hole move independently through their respective bands until they recombine (electron returning to the ground state) or until they fall into a trap (metastable state). If there is instantaneous emission of light owing to these transitions, the phenomenon is called *fluorescence*. If an electron in the trap requires energy to get out of the trap and fall to the valence band, the emission of light in this case is called *phosphorescence* (delayed fluorescence). If phosphorescence at room temperature is

very slow, but can be speeded up significantly with a moderate amount of heating ( $\sim 300^\circ\text{C}$ ), the phenomenon is called *thermoluminescence*.

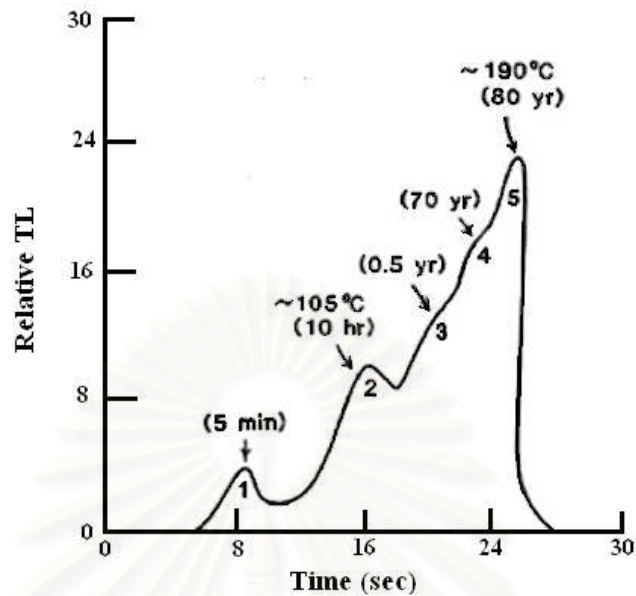


**Figure 2.7** The glow curve of lithium fluoride (TLD-100).

A plot of thermoluminescence against temperature is called a glow curve (figure 2.7). As the temperature of the thermoluminescence material exposed to radiation is increased, the probability of releasing trapped electron increases. The light emitted first increases, reaches a maximum value, and fall again to zero. Because most phosphors contain a number of traps at various energy levels in the forbidden band, the glow curve may consist of a number of glow peaks as shown in figure 2.6. The different peaks correspond to different “trapped” energy levels.

### 2.1.3.2 Lithium fluoride

Lithium fluoride has an effective atomic number of 8.2 compared with 7.4 for soft-tissue. This makes this material very suitable for clinical dosimetry. The dose absorbed in LiF can be converted to dose in muscle by considerations similar to those discussed earlier. For example, under electronic equilibrium conditions, the ratio of absorbed doses in the two media will be the same as the ratio of their mass energy absorption coefficients. If the dimensions of the dosimeter are smaller than the ranges of the electron crossing the dosimeter, then the Bragg-Gray relationship can also be used. The ratio of absorb doses in the two media will the same as the ratio of mass stopping powers. The applicability of the Bragg-Gray cavity theory to TLDs has been discussed by several authors.

### 2.1.3.3 Practical consideration

As stated previously, the TLDs must be calibrated before it can be used for measuring as unknown dose. Because the response of the TLD materials is affected by their previous radiation history and thermal history, the material must be suitably annealed to remove residual effects. The standard pre-irradiation annealing procedure

for LiF is 1 hour of heating at 400°C and then 24 hours at 80°C. The slow heating, namely 24 hours at 80°C, remove peak 1 and 2 of the glow curve by decreasing the trapping 'efficiency'. Peak 1 and 2 can also be eliminated by post-irradiation annealing for 10 minutes at 100°C. The need for eliminating peak 1 and 2 arise from the fact that the magnitude of these peaks decreases relatively fast with time after irradiation. By removing these peaks by annealing, the glow curve becomes more stable and therefore predictable.

The dose response curve for TLD-100 is shown in figure 2.8. The curve is generally linear up to  $10^3$  cGy but beyond this it becomes supralinear. The response curve, however, depends on many conditions that have to be standardized to achieve reasonable accuracy with TLDs. The calibration should be done with the same TLD reader, in approximately the same quality beam and to approximately the same absorbed dose level. The TLD response is defined as thermoluminescence output per unit absorbed dose in the phosphor. Figure 2.10 gives the energy response curve for LiF (TLD-100) for photon energies below megavoltage range. The studies of energy response for photons above  $^{60}\text{Co}$  and high energy electron have yielded somewhat conflicting results.

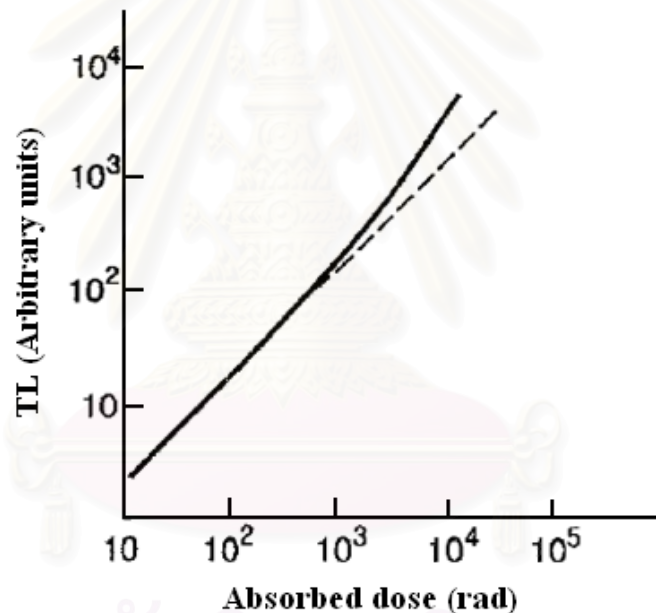


**Figure 2.8** An example of thermoluminescence versus absorbed dose curve for TLD-100 powder.

When considerable care is used, precision of approximately 3 % may be obtained using TLD powder or extruded material. Although not as precise as the ion chamber, TLD's main advantage is in measuring doses in regions where ion chamber cannot be used. For example, TLD is extremely useful for patient dosimetry by direct insertion into tissue or body cavities. Since TLD material is available in many forms and sizes, it can be used for special dosimetry situations such as for measuring dose distribution in the build-up region, around brachytherapy source, and for personal dose monitoring.

### 2.1.3.4 Energy response

The photoelectric absorption process is usually the predominant absorption process at low (< 100 keV) photon energies. This interaction, which involves the innermost electrons, is dependent on the nuclear charge of the atom, the atomic number (Z). Consequently, radiation detectors with high atomic number show a greatly enhanced response at the low photon energies. The energy response of a detector at the particular photon energy may be defined as the response of the detector at that photon energy relative to its response at some reference energy (usually 1-3 MeV) where the photoelectric absorption process is largely inoperative. The dosimeter is said to have a good energy response if its response per roentgen shows little change with photon energy, the energy response is poor if this charge is charge. Detectors with an effective atomic number approximately that of air ( $Z = 7.64$ ) show a good energy response while those with an effective atomic number much different from 7.64 show a poor energy response.

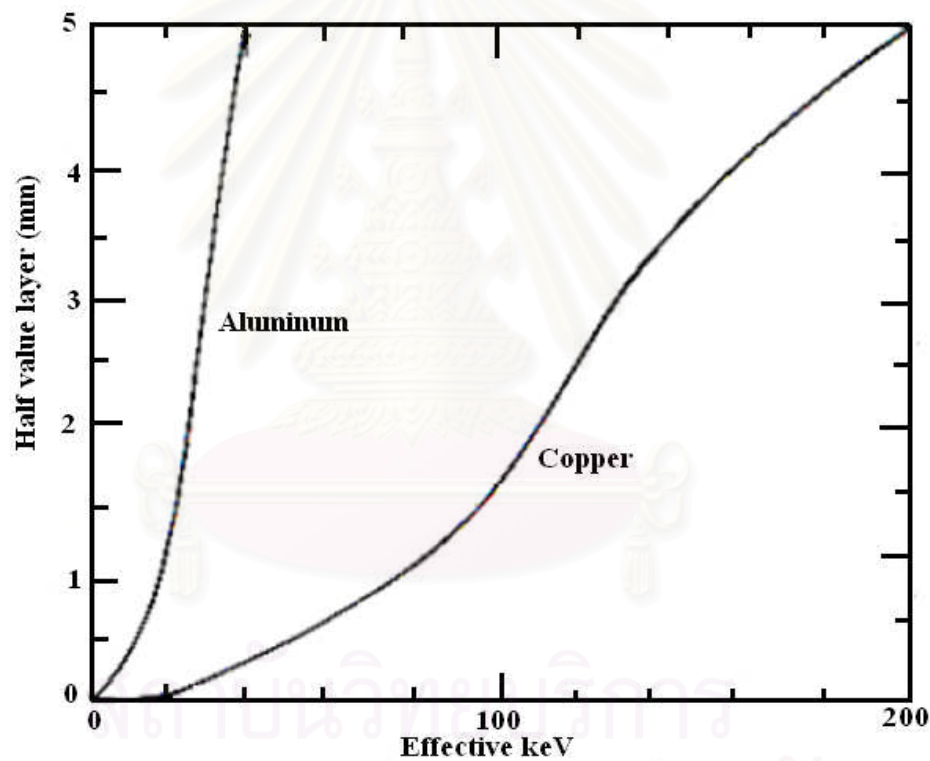


**Figure 2.9** Relation of half value layer to effective energy.

One recurring problem in dealing with energy response is the precise statement of x-ray beam quality. If the radiation source is a monoenergetic gamma-ray emitter (for example,  $^{137}\text{Cs}$ ) then the beam quality can be expressed simply and accurately as the monoenergetic photon energy (662 keV). On the other hand, if the radiation source used in an x-ray generator that produces a spectrum of photon energies up to the maximum accelerating voltage, then specification of the beam quality is much more difficult. Beam quality may be expressed in terms of “effective keV” defined as that monoenergetic photon energy which has the same half value



layer as dose the x-ray beam in question. Conversion from the measured half value layer to effective energy (keV) can be made from figure 2.9. Effective energy determined in this manner is not a highly precise statement of quality for example, two x-ray beams generated at different accelerating voltages and with different filtrations can have identical half value layer (and consequently the same effective energy). It is often valuable to specify the first and second half value layer as well as the accelerating voltage and the amount of filtration.

There are two ways to determine energy response curves for thermoluminescence phosphors by using experimentally determined values based on effective energy for various x-ray and gamma-ray sources or by using theoretically calculated values from available absorption coefficients for the various photon energies. Experimentally measured values are usually more appropriate when correction for the energy responses in various experimental irradiations. Figure 2.10 show energy response curves which were calculated by comparing the absorption coefficients of the various thermoluminescence phosphors with the energy deposited in tissue. Energy response is usually related to the exposure in air rather than to the dose in tissue. ((1)  $\text{CaSO}_4$ ; (2)  $\text{CaF}_2$ ; (3)  $\text{Al}_2\text{O}_3$ ; (4)  $\text{LiF}$ ; (5)  $\text{CaCO}_3$ ; (6)  $\text{SiO}_2$ ; and (7)  $\text{Li}_2\text{B}_4\text{O}_7$ )

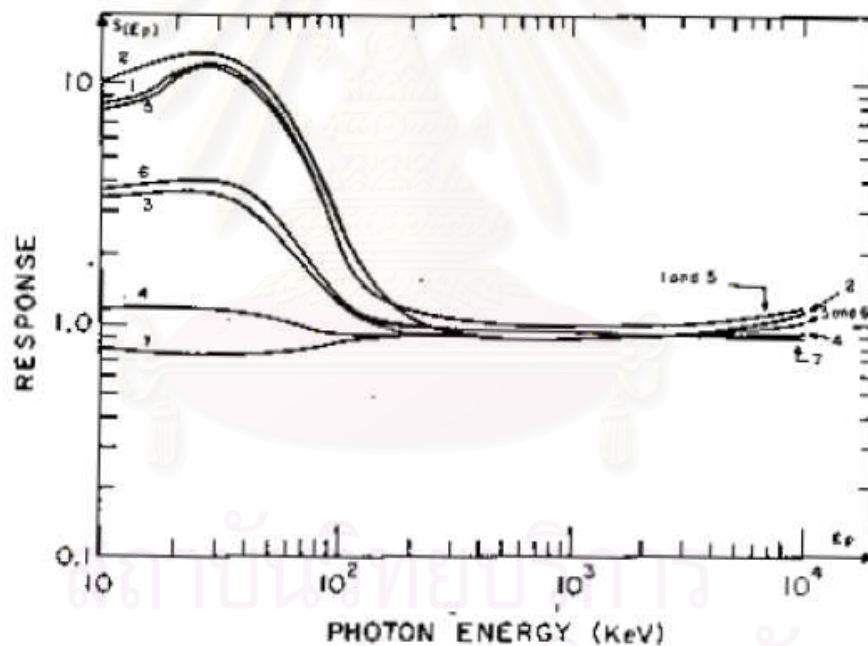


**Figure 2.10** Theoretical sensitivity of thermoluminescence phosphors.

#### 2.1.3.5 Calibration of thermoluminescent dosimeters [10]

The purpose of calibrating a TLD instrument is to produce consistent and accurate reading in dosimetrically meaningful units. The calibration process involves the following 3 steps.

### A) Generate calibration dosimeter

In this process, an element correction coefficient (ECC) is generated by using a set of dosimeters, typically 1 – 2 % of the total population to be calibration dosimeters. They are identified and segregated from the field dosimeters.

All dosimeters are annealed to clear them all residual exposure. Duration time between annealing and exposing should be the same for all dosimeters. After being exposed to the known radiation dose, the charge integral value ( $Q_i$ ) in nanocoulomb (nC) of each dosimeter ( $i$ ) is read out and recorded. Then the average charge integral ( $\bar{Q}$ ) of all dosimeters is calculated and the element correction coefficient ( $ECC_i$ ) for individual dosimeter  $i$  ( $i = 1, 2, 3, \dots, n$ ) is computed by dividing the average charge integral by the individual charge ( $Q_i$ ) as:

$$ECC_i = \frac{\bar{Q}}{Q_i} \quad (2.14)$$

### B) Calibration of thermoluminescent dosimeter reader

A group of dosimeters about 1 – 2 % of dosimeters in (a) which have  $ECC_i$  value close to 1 are chosen to be calibration dosimeters. The calibration dosimeters are exposed to known amount of radiation dose ( $D$ ) in grays and read by TLD reader. As ( $Q_i$ ) is the reading for the dosimeter  $i$ , the corrected charge integral ( $Q_{ci}$ ) of the dosimeter is calculated by:

$$Q_{ci} = Q_i \times ECC_i \quad (2.15)$$

Then the reader calibration factor (RCF) is calculated from the equation:

$$RCF = \frac{\bar{Q}_c}{D} \quad (2.16)$$

When  $\bar{Q}_c$  is the average corrected charge integral and calculated by:

$$\bar{Q}_c = \frac{1}{n} \left( \sum_{i=1}^n Q_{ci} \right) \quad (2.17)$$

### C) Calibration of dosimeter

The rest of the dosimeter [number of the dosimeters in (a) – number of dosimeters in (b)] is used as field dosimeters. They are exposed by the known

radiation dose of  $L$  grays and read by TLD reader. The calibration value of element correction coefficient for individual dosimeter ( $ECC_{ci}$ ) is then calculated by:

$$ECC_{ci} = \frac{(RCF \times L)}{Q_i} \quad (2.18)$$

### 2.1.3.6 Determination of unknown radiation dose

The field dosimeters in 2.1.3.5 (C) are used to measure unknown radiation dose. The unknown dose  $D$  in grays is calculated by using  $ECC_{ci}$  from the equation:

$$D = \frac{(Q_i \times ECC_{ci})}{RCF} \quad (2.19)$$

When  $Q_i$  is the reading of the individual field dosimeter  $i$  of any user defined length.

### 2.1.4 Estimating effective dose from computed tomography

The definition of effective dose was given equation 2.20 [11] as the weighted sum of organ doses resulting from the examination, where the radiosensitive organs were defined along with their tissue-weighting factors. Although it appears straightforward to estimate effective dose, it is actually difficult to accurately estimate the dose to an individual organ from a CT scan. This is even more difficult when attempting to estimate the effective dose for each patient when each one has unique characteristics of height, weight, age, gender, and composition. Still, several different methods for estimating effective dose primarily to standard patient models have been developed.

$$E = \sum_T (w_T \cdot w_R \cdot D_{T,R}) \quad (2.20)$$

where  $E$  is the effective dose,  $w_T$  is the tissue-weighting factor,  $w_R$  is the radiation-weighting coefficient (1 for x-ray),  $D_{T,R}$  is the average absorbed dose to tissue T, T is the subscript for each radiosensitive tissue, and R is the subscript for each type of radiation (here, only x-rays are present). The weighting factors are set for each radiosensitive organ in Publication 60 of the International Commission on Radiological Protection (ICRP) [11]. Effective dose is measured in sieverts (Sv) or rems. The conversion between sieverts and rems is  $100 \text{ rem} = 1 \text{ Sv}$ .

The first is based on Monte Carlo simulations performed several years ago [12]. This work, performed by members of the United Kingdom's National Radiological Protection Board (NRPB), used Monte Carlo methods to simulate CT

scanning around a previously developed mathematical patient model (MIRD V [13]). This hermaphrodite patient model uses geometric shapes (cylinders, spheres, cones) to approximate the shape and location of all radiosensitive organs in the body: other approximations were used for the brain and lens of the eye. Physical measurements of CTDI in air on many scanners were collected as part of a national dosimetry program [14]; these data were used to convert from the normalized Monte Carlo data to absolute dose values. The simulation also involved modeling scanner geometry, spectrum, section thickness, and other properties with the patient model in the beam accounting for primary and scatter radiation. From these simulations, radiation doses for each organ in each imaged section were calculated and could be tallied to estimate the organ dose for each organ. These organ doses could then be combined with appropriate weighting factors to estimate effective dose (or effective dose equivalent from ICRP 26). This work was completed before helical and multi detector scanners were commonplace and did not explicitly model helical scanning or the effects of multi detector scanners.

The work formed the basis for several software programs that have taken the results of these simulations and put an interface on them to allow users to input some technical parameters and calculate an effective dose. These include programs such as CTDOSE (from John Le Heron at New Zealand's National Radiation Laboratory [[johnleh@nrl.moh.govt.nz](mailto:johnleh@nrl.moh.govt.nz)]) and the Microsoft (Redmond, Wash) Excel-based product from the Imaging Performance Assessment of CT (ImPACT) scanners group in the United Kingdom [15]. The latter software package matches the desired scanner to one of those used in the original study on the basis of CTDI in air as well as CTDI in phantom measurements.

### 2.1.5 ImPACT dose survey

The dosimetry used in the 1989 NRPB survey was based on Monte Carlo simulations [16] of calculated x-ray spectra in an adult, hermaphrodite, mathematical phantom, it is shown in figure 2.11.

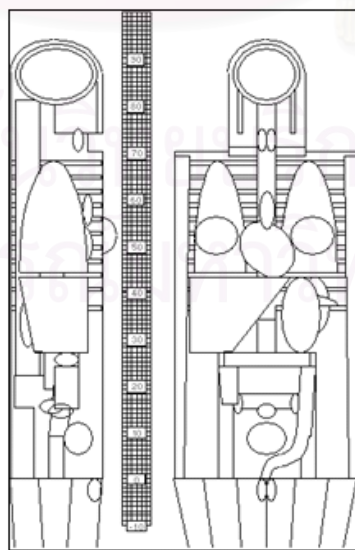


**Figure 2.11** Mathematical phantom.

The free-in-air, on-axis dose was measured for each scanner and, with knowledge of kV, focus-to-axis distance and details of the x-ray beam filter (figure 2.12), the Monte Carlo techniques modeled the dose distribution within the mathematical phantom. In total, 23 data sets were produced for all the surveyed scanner models. Doses in the data sets are obtained from the simulated, individual irradiation of 208 contiguous, 5 mm thick transverse slabs, covering the mathematical phantom [3]. A data set therefore consists of 208 normalized dose values for each of the 27 organs or regions represented in the phantom.

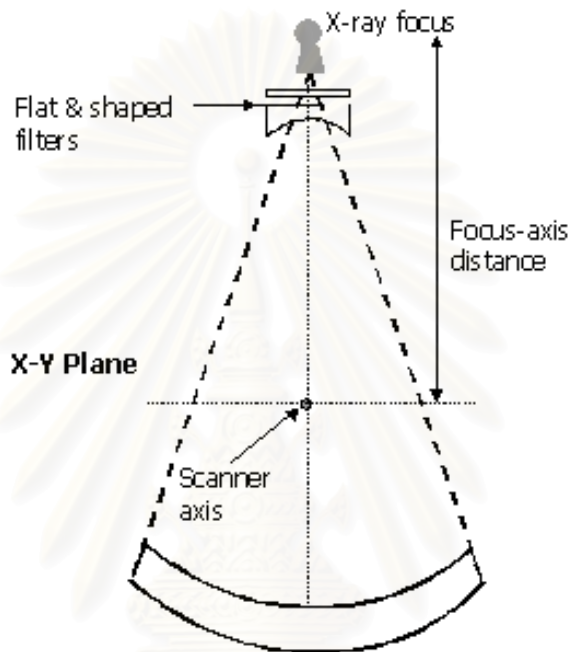


**Figure 2.12** The dose distribution of a computed tomography scanner.

After publication of the NRPB survey data, a computer data package, CTDOSE [17], was made available. This software requires an input of scanner model, kV and scan type (head/body), to select the appropriate NRPB Monte Carlo data set. With additional information on scanning parameters, such as mAs, slice width, number of slices, scan start position and couch increment, it utilizes the normalized organ dose data to provide a listing of the organ doses and effective dose for the required examination.

In 2000 over half the existing scanners in the UK were models not covered by the 1989 NRPB survey, therefore difficulties arise when attempting to estimate doses from this equipment. ImPACT chose to tackle this problem by determining a method of "matching" the dosimetric characteristics of the new scanner models to those scanner models covered by the NRPB data sets ("NRPB" scanners). In this way, a new scanner model can be matched to an existing NRPB Monte Carlo data set that describes its dose distribution. With funding provided by the Department of Health Safety Division, a dose survey was planned with the aim of collecting data on all current CT scanners, including those in the NRPB survey. In April 1997 a round-table meeting was held at St George's Hospital to discuss and establish the survey protocol. The meeting was attended by approximately 40 physicists, representing 30 centers in

the UK and Europe [18]. A protocol was subsequently finalized to measure the following parameters: x-ray beam quality (determined by half-value layer); x-ray filter shape (measurement of in-air output across the scan plane) and computed tomography dose index (CTDI on-axis, free-in-air, and at the center and periphery of standard head and body dose phantoms). The data from the survey was centrally collated by ImPACT. Information was obtained on a total of 75 scanners from 35 centers in the UK and Europe. The results were checked for accuracy and consistency, and any anomalous data was excluded.

The ImPACT survey data were used to determine which of the measured parameters was most closely related to patient dose. This was done by correlating the measurements from the NRPB scanners with the effective doses calculated using the CTDOSE software.

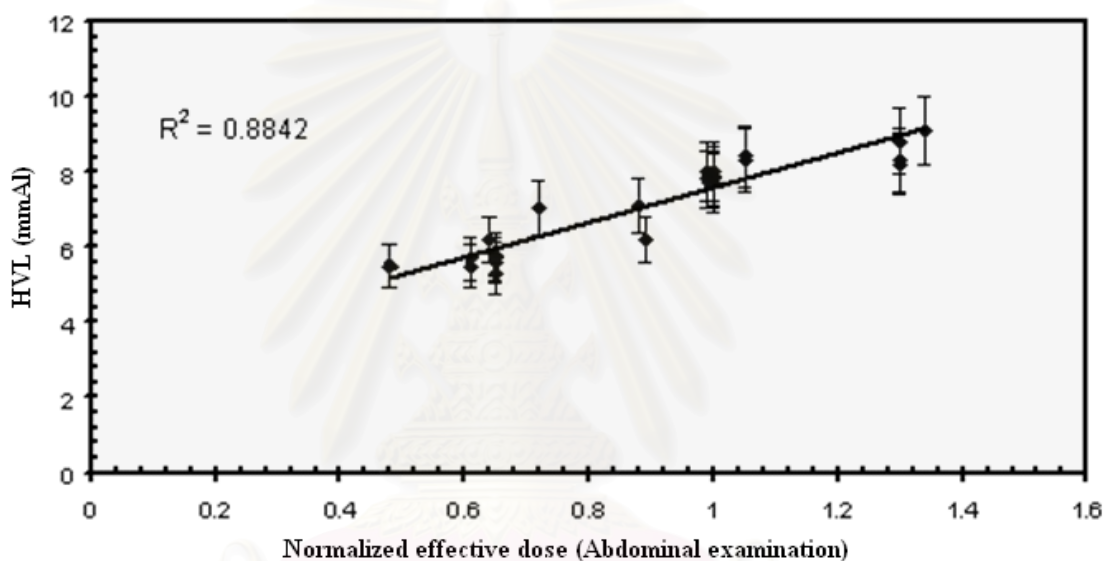


**Figure 2.13** Correlation of x-ray beam half-value layer and normalized effective dose for abdominal examinations.

Figure 2.13 shows an example of the correlation between effective dose (normalized to on-axis, in-air dose) and x-ray beam half-value layer. Although a reasonable correlation is obtained with this single parameter, it was found that a better predictor of effective dose was a combination of the ratios  $CTDI_{center}/CTDI_{air}$  and  $CTDI_{periphery}/CTDI_{air}$ . This value has been termed the ImPACT Factor (ImF), and its correlation with normalized effective dose, for abdomen examinations, it is shown in figure 2.14.

ImPACT Factors were calculated for all CT models in the ImPACT survey, and each new scanner model matched to an "NRPB" scanner by comparison of ImPACT Factors. This enabled the selection of the appropriate Monte Carlo data set for new scanner models when using the CTDOSE program (or similar software utilizing the NRPB data sets). When a new CT scanner is launched, all that is required to calculate a new ImPACT Factor are the CTDI value in-air and the CTDI values at the centre and periphery of the head and body dose phantoms. For each scanner, at each kV, the ImPACT Factor varies with examination type e.g. head, neck, chest,

abdomen, and pelvis. However, the variation between different head examinations or different body examinations is not significant. Therefore, in order to simplify matching, only two ImPACT Factors are calculated, one to match scanners for head examinations and the other for body examinations.

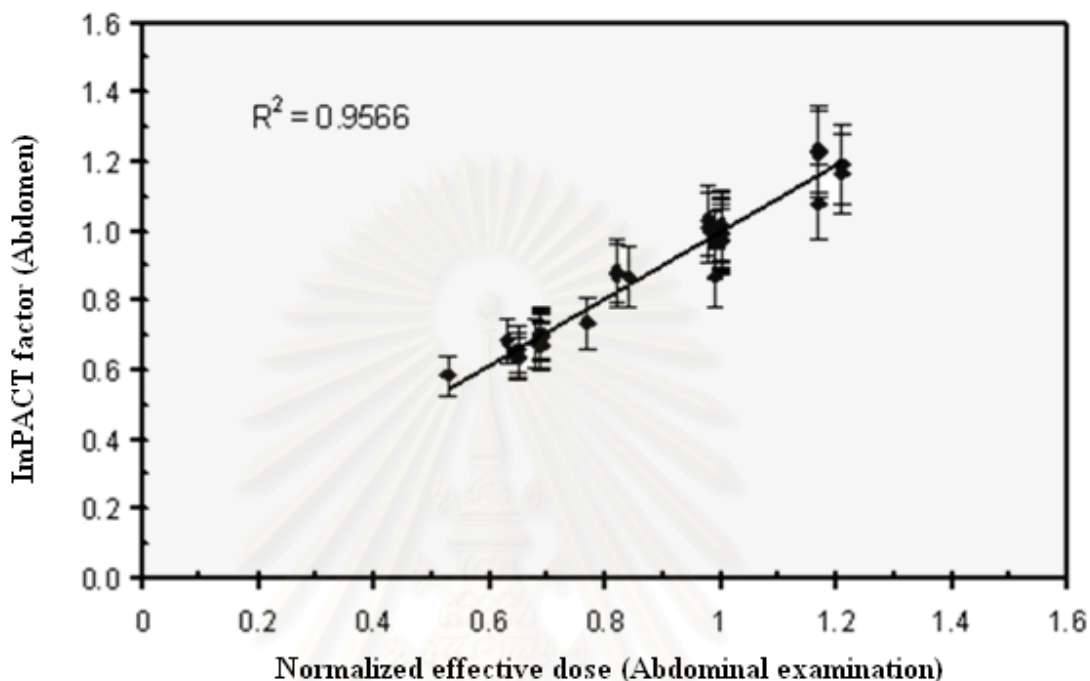


**Figure 2.14** Correlation of ImPACT factor and normalized effective dose for abdominal examinations.

As a result of the ImPACT CT dose survey, it is now possible to estimate patient doses from CT examinations for over 90% of scanners currently installed in the UK. The full list is available on the ImPACT web-site, [www.impactscan.org](http://www.impactscan.org), and is regularly updated as CTDI data on new scanner models becomes available.

## 2.1.6 The ImPACT program

### 2.1.6.1 Introduction

This spreadsheet is a tool for calculating patient organ and effective doses from CT scanner examinations. It makes use of the NRPB Monte Carlo dose data sets produced in report SR250. SR250 provides normalized organ dose data for irradiation of a mathematical phantom by a range of CT scanners. As SR250 was produced in 1993, it does not include data for more modern scanners. To overcome this problem, the ImPACT CT scanner dose survey was carried out by physicists in the UK and Europe. This work provides a method for 'matching' the dose distribution of newer scanners to scanners included in SR250. The matching results are included in this spreadsheet. As new scanners are introduced, their matches will be included in updates to this spreadsheet.

### 2.1.6.2 Installation

The system should work on any PC with Microsoft Excel 2000 or above. It has not yet been tested on an Apple computer, but it is anticipated that it should work on a Mac. Installation is fairly simple, and only requires the SR250 data sets (MCSET01.DAT to MCSET23.DAT) to be present in the same directory as this spreadsheet (SR250 is sold by the NRPB). Macros are used on this spreadsheet for a variety of purposes. Depending on your version of Excel, and macro options, the security level may have to be switched to 'medium' (select 'Tools' -> 'Options' -> 'Security' -> 'Macro Security'), and/or ImpACT added to your trusted Macro sources. This spreadsheet has been checked for macro viruses, and the logic and calculations been tested extensively, however ImpACT accept no responsibility for loss or damage incurred as a result of its use.

**ImpACT CT Patient Dosimetry Calculator**  
Version 0.99x 20/01/06

Scanner Model:			
Manufacturer:	CGR		
Scanner:			
KV:			
Scan Region:	Head		
Data Set:	#N/A	Update Data Set	
Current Data:	MCSET00		
Scan range			
Start Position:	0	cm	Get From Phantom Diagram
End Position:	44	cm	
Patient Sex:	f		

Acquisition Parameters:			
Tube current:			mA
Rotation time:			s
mAs / Rotation:	0		mAs
Collimation:			mm
Slice Width:			mm
Pitch:			
Rel. CTDI:	Look up	1.00	(assumed)
CTDI (air):	Look up	#N/A	mGy/100mAs
CTDI (soft tissue):	#N/A		mGy/100mAs
$CTDI_w$ :	Look up	#N/A	mGy/100mAs

Organ	$w_T$	$H_T$	$w_T H_T$
Gonads	0.2	#N/A	#N/A
Bone Marrow (red)	0.12	#N/A	#N/A
Colon	0.12	#N/A	#N/A
Lung	0.12	#N/A	#N/A
Stomach	0.12	#N/A	#N/A
Bladder	0.05	#N/A	#N/A
Breast	0.05	#N/A	#N/A
Liver	0.05	#N/A	#N/A
Oesophagus (Thymus)	0.05	#N/A	#N/A
Thyroid	0.05	#N/A	#N/A
Skin	0.01	#N/A	#N/A
Bone Surface	0.01	#N/A	#N/A
#N/A	0.025	#N/A	#N/A
Remainder 2	0.025	#N/A	#N/A
<b>Total Effective Dose (mSv)</b>			<b>#N/A</b>

Remainder Organs	$H_T$
Adrenals	#N/A
Brain	#N/A
Upper Large Intestine	#N/A
Small Intestine	#N/A
Kidney	#N/A
Pancreas	#N/A
Spleen	#N/A
Thymus	#N/A
Uterus	#N/A
Muscle	#N/A

$CTDI_w$ (mGy)	#N/A
$CDTI_{vol}$ (mGy)	#N/A
DLP (mGy.cm)	#N/A

© nk for ImpACT, 2000-2005  
Imaging Performance Assessment of CT Scanners, an MHRA Evaluation centre  
<http://www.impactscan.org>

Figure 2.15 The ImpACT program.



### 2.1.6.3 Worksheet

CTDosimetry.xls consists of 12 worksheets:

1. Introduction: Provides an introduction and instructions for use
2. Scan Calculation: The data entry and results sheet
3. Pediatric: Information on relative doses to adult and pediatric patients
4. Phantom: Allows interactive selection of the scan range used for dose calculation using a diagram of the phantom used to generate SR250
5. Scanners: Provides data on CT scanner models, including CTDI in air and phantom, as well as the scanner matching data
6. Match Data: Gives data required to perform the scanner matching in the Scanners worksheet
7. Collimation: Lists relative CTDI values at different collimations for a range of CT scanners. These values are more useful for multi-slice scanners, as the CTDI can vary considerably over the range of available collimations
8. Monte Carlo Data: Contains the unformatted SR250 data set
9. Doses: Contains the formatted dose data from the SR250 data set that is currently loaded
10. Dose Calculations: Performs the organ dose calculations, and calculation of remainder organ doses etc
11. Selections: Provides data for the drop down selection boxes in the Scan Calculation worksheet, and performs calculations for 'remainder' organ doses
12. Version: Details changes made in each version, from version 0.99e onwards

There are also a number of Visual Basic macros used by CTDosimetry.xls, held in the modules Phantom Diagram, Scanner Selection and Update Data Set.

### 2.1.6.4 Using CTDosimetry.xls

To calculate doses using CTDosimetry.xls, the user must enter a number of parameters relating to the scanner and the scan series. The following four selections, made in the top left box on the Scan Calculations worksheet define the Monte Carlo data set that is used:

1. Manufacturer: Select the scanner manufacturer from the drop down list
2. Scanner: Select the scanner model or scanner model group for the drop down list
3. kV: Choose the appropriate scan kV
4. Scan Region: Choose head or body

The Monte Carlo data set that is used for this combination of scanner, kV and body part is displayed in the cell marked 'Data Set'. The data set that is currently loaded is displayed below. If these do not match, no dose is calculated. To load the appropriate data set, and enable dose calculation, press the 'Update Data Set' button.

Scan and patient data is entered in the box on the top right of the Scan Calculations worksheet:

5. mA: The x-ray tube current. Note that this should be the actual scanner mA, and not the 'effective mAs' displayed on some multi-slice scanners

6. Rotation time: The scanner tube rotation time
7. mAs/rotation: Do not enter data in this box (it is calculated automatically)
8. Collimation: The total nominal x-ray beam width along the z-axis, selected from a range of possible values in the drop down box. This determines the relative CTDI compared to the reference (usually 10 mm) collimation.
9. Slice width: The scanner collimation slice width that is not actually used in calculations, but can be useful in printed output
10. Pitch: The scanning pitch (table travel per rotation/total collimated slice width). For axial scanning, (couch increment)/(collimated slice width) should be used
11. Rel. CTDI: The CTDI at the selected collimated x-ray beam thickness, relative to the CTDI at the reference collimation (usually 10 mm)
12. CTDI (air): The free in air CTDI100 value (in mGy/100mAs), as defined in EUR 16262: European Guidelines on Quality Criteria for Computed Tomography, pub, European Commission. CTDI values for most of the scanners are listed on the Scanner Worksheet. Pressing the 'Look up' button will enter the value in this cell. The value in this cell is corrected for the relative CTDI value in the cell above
13. CTDI (soft tissue): The CTDI to ICRU muscle, used as an approximation to the dose to soft tissue within the body. This is the CTDI(air) x 1.07 for CT scanner energies
14.  $n$ CTDI<sub>w</sub>: Weighted CTDI<sub>w</sub> measured in a standard CTDI phantom (normalized for 100 mAs).  $CTDI_w = 1/3CTDI_{center} + 2/3 CTDI_{periphery}$
15. Patient Sex: Enter 'm' or 'f' in this cell for male or female patients. This affects the organ used for gonad dose calculation. If left blank, the program will use an average value
16. Start Position: The start position of the scan series. The diagram on the Phantom worksheet shows the position of the phantom's organs relative to the number scale, which is 0 at the base of the trunk. This value can be entered manually in the worksheet, or can be taken from the shaded area on the Phantom worksheet diagram. This can be adjusted using the up and down arrows. Pressing the 'Get From Phantom Diagram' button enters these values into the start and end position boxes in Scan Calculation
17. End Position: The end position of the scan series - Note that this should include the slice thickness, so, for example, a single 5mm slice 20cm from the base of the trunk would have a start position of 20, and an end position of 20.5cm. Start and End position values are interchangeable

When the above values are entered, the doses to each of the individual organs, as defined by the SR250 data set appear in the cells below the scan parameters. These are combined according to the tissue weighting factors given in ICRP60, to calculate an effective dose. In addition, the weighted CTDI (CTDI<sub>w</sub>), volume CTDI<sub>w</sub> (CTDI<sub>vol</sub>) and dose length product (DLP) are also displayed.

Note that not all of the ICRP60 organs are included in NRPB SR250. In order to estimate dose to the esophagus, the thymus dose is used. The dose for muscle is approximated from the total body dose - dose to all other organs and contents.

## 2.2 Literature review

Groves AM et al [19] studied the computer simulations which are widely used to estimate effective doses from CT examinations. The raw data often used in their estimations were obtained some years ago and made certain assumptions regarding CT unit design. At that time multidetector CT units were unavailable. Changes in design will limit the accuracy of computer simulated dosimetry on these machines. They therefore estimated CT dose on a 16-detector unit directly using TLDs and an anthropomorphic phantom. They found that the dose measured directly was 18% higher than the computer simulated dosimetry.

Geleijns J et al [20] studied Comparison of two methods for assessing patient dose from computed tomography. The organ doses determined using two methods and these served as a basis to calculate the effective dose. Thermoluminescence dosimeters were used to measure organ doses in an anthropomorphic Rando Alderson phantom. In addition organ doses were obtained from measurement of the computed tomography dose index and the application of published organ dose conversion factors. Effective dose values obtained with the Rando phantom for CT head examinations are about 1-2 mSv. For CT examinations of thorax and abdomen the estimation of effective doses with the Rando phantom yielded values of 18 and 24 mSv respectively. Effective doses determined from CTDI values were similar for CT head examinations (1-2 mSv) but were smaller for the CT thorax scan (11-15 mSv) and the CT abdomen scan (15-20 mSv). In their study effective dose values are relatively high compared with the results of other investigators who indicate effective doses and effective dose equivalents of 7-9 mSv for CT of the thorax and of 4-16 mSv for CT of the abdomen. Discrepancies between their results and those from other studies could be attributed to differences in the selected CT protocols and to differences in the phantoms employed.

Janeczek J et al [21] studied the measurement of CT scanner radiation dose profile using thermoluminescent dosimeters. Thermoluminescence detectors in the form of thin discs were used for dose profile measurement of CT scanners CT/T8800, CT9800 and CT MAX made by General Electric, CT 1200 SX made by Picker and SOMATOM 2 made by Siemens. Effective energy of a CT scanner x-ray was evaluated prior to calibration and measurement. Dose profiles of all nominal slice thicknesses down to 1.5 mm and of a multiple scan were measured for each CT scanner. CT dose indexes were derived from the dose profiles and compared with values measured by a pencil type ionization chamber.

McNitt-Gray MF [6] described basic radiation dose concepts as well as those specifically developed to describe the radiation dose from computed tomography. Basic concepts of radiation dose were reviewed, including exposure, absorbed dose, and effective dose. Radiation dose from CT demonstrated variations within the scan plane and along the z axis because of its unique geometry and usage. Several CT specific dose descriptors have been developed: the multiple scan average dose descriptor, the computed tomography dose index and its variations ( $CTDI_{100}$ ,  $CTDI_w$ ,  $CTDI_{vol}$ ), and the dose-length product. Factors that affect radiation dose from CT include the beam energy, tube current-time product, pitch, collimation, patient size, and dose reduction options. Methods of reducing the radiation dose to a patient from CT include reducing the milliampere-seconds value, increasing the pitch, varying the milliampere-seconds value according to patient size, and reducing the beam energy. The effective dose from CT can be estimated by using Monte Carlo methods to simulate CT of a mathematical patient model, by estimating the energy imparted to

the body region being scanned, or by using conversion factors for general anatomic regions. Issues related to radiation dose from CT are being addressed by the Society for Pediatric Radiology, the American Association of Physicists in Medicine, the American College of Radiology, and the Center for Devices and Radiological Health of the Food and Drug Administration.

Hashemi-Malayeri B et al [22] studied a practical method for the assessment of patient doses from computed tomography scanners. In the presentation the significance of the radiation dose associated with computed tomography was reviewed. Then the most common CT dosimetry approaches and the framework of their practical direct dosimetry approach are presented. Finally the results of applying our developed direct dosimetry method along with the Monte Carlo method for one model of CT scanners will be presented and compared with each other. The effective dose values for Philips Tomoscan CX/S CT Scanner, the direct method indicated a value of up to 50% higher than the Monte Carlo method for most of the CT examinations.



สถาบันวิทยบริการ  
จุฬาลงกรณ์มหาวิทยาลัย

# CHAPTER 3

## RESEARCH METHODOLOGY

### 3.1 Research design

This study is an observational research.

### 3.2 Research design model

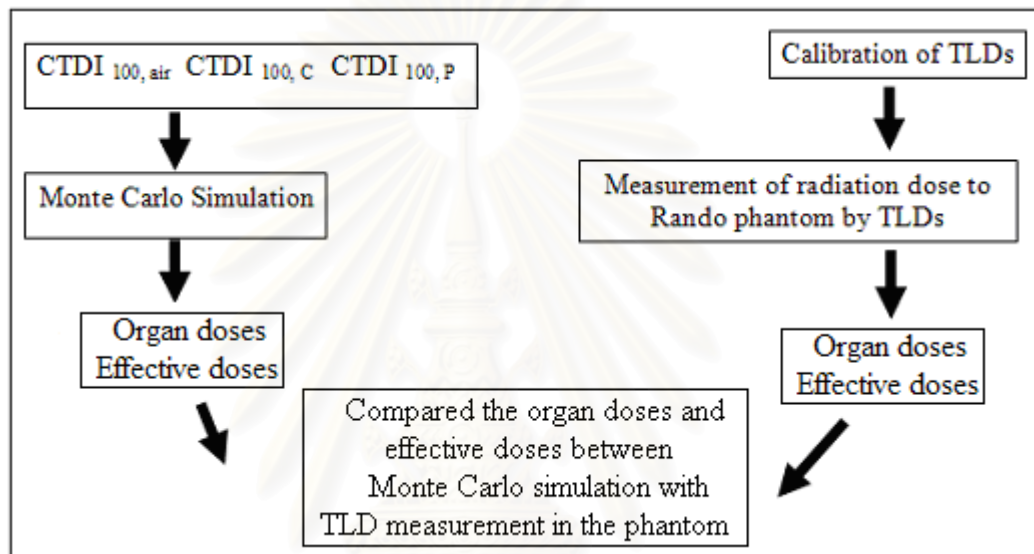


Figure 3.1 Research design model.

### 3.3 Conceptual framework

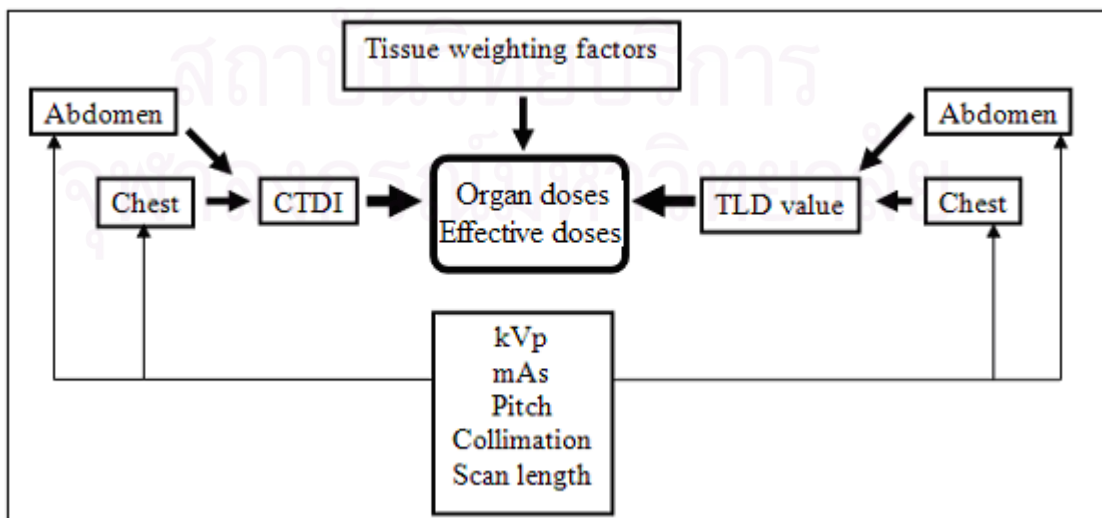


Figure 3.2 Conceptual framework.

### 3.4 Keywords

- Effective dose
- Computed tomography
- Monte Carlo simulation
- Thermoluminescent dosimetry

### 3.5 Research question

How much is the difference of effective dose between estimation from Monte Carlo simulation and thermoluminescent dosimetry for the phantom undergo the computed tomography examinations?

### 3.6 Materials

#### 3.6.1 The pencil ionization chamber

The 100 mm long pencil ionization chamber: DCT 10-RS S/N 1057 [23] is shown in figure 3.3. It has 4.9 cm<sup>3</sup> active volumes, 10 cm total active length, 0.8 cm inner diameter of outer electrode, and 0.1 cm diameter of inner electrode. It is connected with the electrometer during the measurement.



**Figure 3.3** The pencil ionization chamber.

### 3.6.2 The electrometer

The electrometer: RTI Electronics AB Type SOLIDOSE 400 Electrometer S/N 4103 [23] is shown in figure 3.4, its leakage is within  $4 \times 10^{-15}$  Amperes for 80 - 150 kV radiation quality, and the calibration factor  $N_{D,K}$  equals to 24.2 mGy cm/nC (120 kV/HWD 4.05 mmAl).

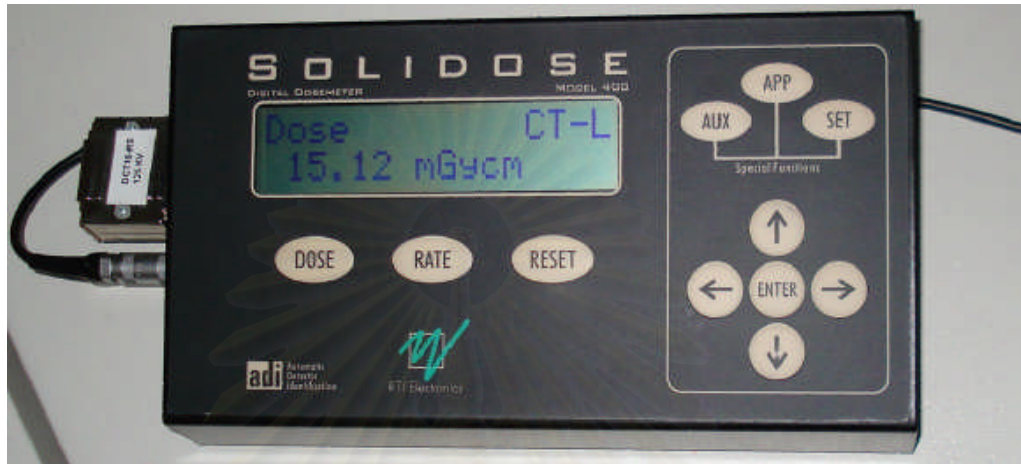


**Figure 3.4** The electrometer.

### 3.6.3 Monte Carlo simulation program

Dose estimation methodology was based on the NRPB Monte Carlo simulations. The exposure factors were entered into the ImpACT spreadsheet [24], along with CTDI which the measurements made with an ionization chamber. The spreadsheet used these data and table of normalized organ doses to estimate the organ dose by matching with the manufacturer CT machine.

ImpACT CT Patient Dosimetry Calculator			
Version 0.99x 20/01/06			
<b>Scanner Model:</b>			
Manufacturer:	CGR		
Scanner:			
kV:			
Scan Region:	Head		
Data Set	#N/A		Update Data Set
Current Data	MCSET00		
<b>Scan range</b>			
Start Position	4	cm	Get From Phantom Diagram
End Position	44	cm	Diagram
Patient Sex:	f		
<b>Acquisition Parameters:</b>			
Tube current	100		mA
Rotation time	1		s
mAs / Rotation	100		mAs
Collimation			mm
Slice Width			mm
Pitch	1.2		
Rel. CTDI	Look up	1.00	(assumed)
CTDI (air)	Look up	#N/A	mGy/100mAs
CTDI (soft tissue)	Look up	#N/A	mGy/100mAs
$n$ CTDI <sub>w</sub>	Look up	#N/A	mGy/100mAs

**Figure 3.5** The ImpACT spreadsheet.

### 3.6.4 The body phantom

The body phantom is shown in figure 3.6, it has 32 cm diameter CTDI PMMA phantom. The 10 cm long CT pencil ionization can be placed in the holes of phantom.



**Figure 3.6** The body phantom.

### 3.6.5 The computed tomography equipment

The Siemens Sensation 16 CT scanner is shown in figure 3.7. The Siemens Sensation 16 is the 7<sup>th</sup> generation multi slice helical CT scanner, featuring a 60 kW generator, 5.3 MHU tube and a fastest gantry rotation time of 0.42 seconds. In helical mode it is capable of imaging 16 slices per rotation, with slice widths of 16 x 1.5 mm and 16 x 0.75 mm, as well as smaller numbers of wider slices. It has 24 parallel rows of solid-state detectors, covering 24 mm in the z direction at the isocenter.



**Figure 3.7** The computed tomography equipment.



### 3.6.6 The Alderson Rando phantom

The Alderson Rando phantom which is shown in figure 3.8 incorporates materials to simulate various body tissue-muscle, bone, lung, and air cavities. It is made of tissue equivalent material based on a synthetic isocyanate rubber. The phantom material is processed chemically and physically to achieve a density of  $0.985 \text{ g/cm}^3$  and an effective atomic number of 7.3 based on the International Commission on Radiation Units and Measurement (ICRU) [25]. The phantom is shaped into a human torso and is sectioned transversely into slices of 2.5 cm each containing a matrix of 0.5 cm diameter holes spaced 3 cm apart. The lungs and cavities are molded of an air-expanded version of the soft tissue material having a density of  $0.3 \text{ g/cm}^3$  and an effective atomic number is the same as soft tissue [26].



**Figure 3.8** The Alderson Rando phantom.

### 3.6.7 The thermoluminescent dosimeters

The TLD used in this study is Lithium Fluoride (LiF) crystal doped with magnesium and titanium (LiF:Mg,Ti). It is known as TLD-100, it consists of Li-6 (7.5%) and Li-7 (92.5%). The TLDs have a nominal density of  $2.64 \text{ g/cm}^3$  and effective atomic number ( $Z_{eff}$ ) of 8.2, a value close to tissue. TLD chips with the dimension of  $3.2 \text{ mm} \times 3.2 \text{ mm} \times 0.89 \text{ mm}$  are used for this study. They are shown in figure 3.9 (left).

Three pieces of TLD chips were loaded in the plastic tubes, shown in figure 3.9 (right). These tubes with TLDs were irradiated for TLD characteristic study and dose measurement.

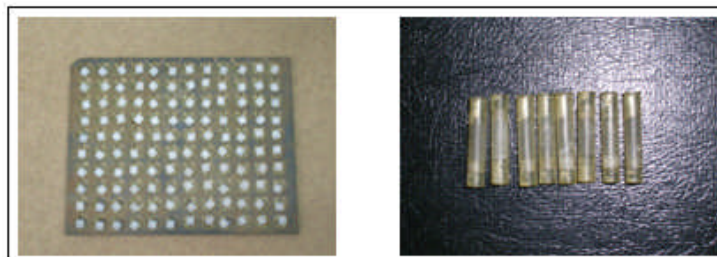


**Figure 3.9** The thermoluminescent dosimeters and plastic tubes.

### 3.6.8 The automatic thermoluminescent dosimeter reader [10]

The Harshaw model 5500 automatic thermoluminescent dosimeter reader is shown in figure 3.10, it is a personal computer driven, table-top instrument for TLD measurement. This reader is capable of reading 50 diameters per loading and accommodates TLD chips, rods and cubes in a variety of sizes. The reader uses hot nitrogen gas heating with a closed loop feedback system that produces linearly ramped temperatures accurate within  $\pm 1^\circ\text{C}$  to  $400^\circ\text{C}$ . Nitrogen is routed through the photomultiplier tube chamber to eliminate condensation.



**Figure 3.10** The automatic thermoluminescent dosimeter reader.

### 3.6.9 The cobalt-60 teletherapy machine

The ELDORADO 78  $^{60}\text{Co}$  source is produced by irradiating ordinary stable  $^{59}\text{Co}$  with neutrons in a reactor. The nuclear reaction can be represented by  $^{59}\text{Co} (n, \gamma) ^{60}\text{Co}$ . The ELDORADO 78 cobalt-60 teletherapy machine is shown in figure 3.11. The source skin distance is 80 cm. The dose rate during the time of study is 25.44 - 26.30 cGy/min at 80 cm SSD.

The  $^{60}\text{Co}$  source decays to  $^{60}\text{Ni}$  with the emission of beta particles ( $E_{\text{max}} = 0.32$  MeV) and two photons per disintegration of energies 1.17 and 1.33 MeV. These gamma rays constitute the useful treatment beam. The beta particles are absorbed in the cobalt metal and stainless-steel capsules. Because of the constant emission of the radiation,  $^{60}\text{Co}$  is used for TLD absorbed dose calibration.



**Figure 3.11** The cobalt-60 teletherapy machine.

### 3.6.10 Water phantom

Basic dose distribution data are usually measured in a water phantom, which closely approximates the radiation absorption and scattering properties of muscle and other soft tissue. Another reason for the choice of water as a phantom material, however, poses some practical problems when used in conjunction with ionization chambers and other detectors that are affected by water, unless they are designed to be waterproof. In most cases, however the detector is encased in a thin plastic (water equivalent) steeve before immersion into the water phantom. The water phantom is shown in figure 3.12.

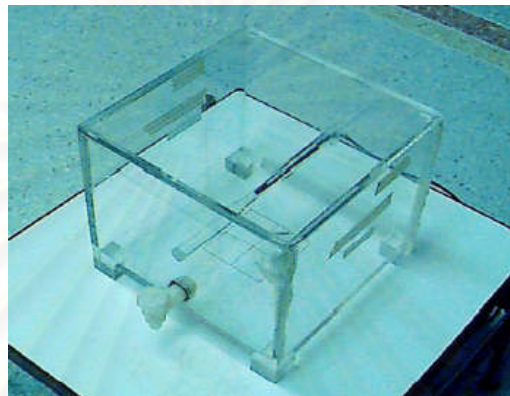


**Figure 3.12** Water phantom.

## 3.7 Methods

The study was performed in department of radiology at King Chulalongkorn Memorial Hospital. This study carried into two parts:

Part 1: Monte Carlo simulation method

Part 2: Thermoluminescent dosimetry method

The quality control of the Siemens Sensation16 CT equipment was undertaken, before performing the dose measurements. The procedures are shown in appendix B.

### 3.7.1 Monte Carlo simulation method

#### 3.7.1.1 Computed tomography dose index measurement

The scan technique was 120 kVp, 100 mAs, 10 mm slice width, 2 x 5 mm collimator, and 350 mm FOV.

A) The pencil chamber was placed in air at the isocenter of gantry. It is shown in figure 3.13.

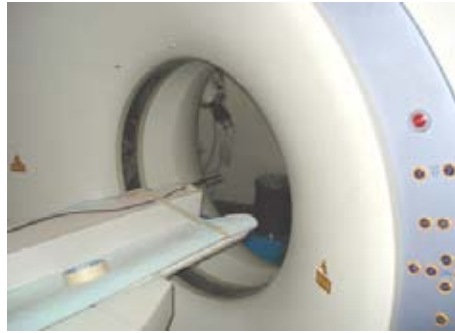


**Figure 3.13** The pencil chamber at the isocenter in air.

- B) The pencil chamber was placed at the center of the body phantom. It is shown in figure 3.14.



**Figure 3.14** The pencil chamber at the center of the body phantom.

- C) The pencil chamber was placed at the peripheries of the body phantom. It is shown in figure 3.15, (a) at 12 o'clock, (b) at 3 o'clock, (c) at 6 o'clock, (d) at 9 o'clock.

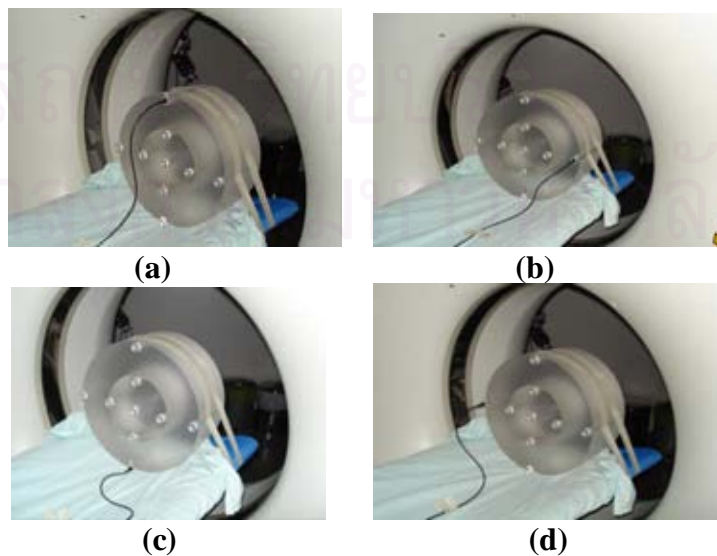


**Figure 3.15** The pencil chamber at the peripheries of the body phantom.

### 3.7.1.2 Simulation the effective dose

The reading values and parameters (kVp, mAs, slice width, collimation, and scan length) were inserted in the ImPACT spreadsheet program to get the effective doses.

**ImPACT CT Patient Dosimetry Calculator**  
Version 0.99x 20/01/06

Scanner Model:			
Manufacturer:	CGR		
Scanner:			
kV:			
Scan Region:	Head		
Data Set	#N/A	Update Data Set	
Current Data	MCSET00		
Scan range			
Start Position	0	cm	Get From Phantom
End Position	44	cm	Diagram
Patient Sex:	f		

Acquisition Parameters:			
Tube current			mA
Rotation time			s
mAs / Rotation	0		mAs
Collimation			mm
Slice Width			mm
Pitch			
Rel. CTDI	Look up	1.00	(assumed)
CTDI (air)	Look up	#N/A	mGy/100mAs
CTDI (soft tissue)		#N/A	mGy/100mAs
$nCTDI_w$	Look up	#N/A	mGy/100mAs

Organ	$w_T$	$H_T$	$w_T H_T$
Gonads	0.2	#N/A	#N/A
Bone Marrow (red)	0.12	#N/A	#N/A
Colon	0.12	#N/A	#N/A
Lung	0.12	#N/A	#N/A
Stomach	0.12	#N/A	#N/A
Bladder	0.05	#N/A	#N/A
Breast	0.05	#N/A	#N/A
Liver	0.05	#N/A	#N/A
Oesophagus (Thymus)	0.05	#N/A	#N/A
Thyroid	0.05	#N/A	#N/A
Skin	0.01	#N/A	#N/A
Bone Surface	0.01	#N/A	#N/A
#N/A	0.025	#N/A	#N/A
Remainder 2	0.025	#N/A	#N/A
<b>Total Effective Dose (mSv)</b>			<b>#N/A</b>

Remainder Organs	$H_T$
Adrenals	#N/A
Brain	#N/A
Upper Large Intestine	#N/A
Small Intestine	#N/A
Kidney	#N/A
Pancreas	#N/A
Spleen	#N/A
Thymus	#N/A
Uterus	#N/A
Muscle	#N/A

$CTDI_w$ (mGy)	#N/A
$CTDI_{vol}$ (mGy)	#N/A
DLP (mGy.cm)	#N/A

**Figure 3.16** The ImPACT spreadsheet program.

สถาบันวิทยบริการ  
จุฬาลงกรณ์มหาวิทยาลัย

ImPACT CT Patient Dosimetry Calculator			
Version 0.99x 20/01/06			
<b>Scanner Model:</b>			
Manufacturer:	Siemens		<b>1</b>
Scanner:	Siemens Sensation 16		<b>2</b>
kV:	120		<b>3</b>
Scan Region:	Body		<b>4</b>
Data Set	MCSET23	Update Data Set	
Current Data	MCSET23	<b>12</b>	
<b>Scan range</b>			
Start Position:	35	cm	<b>5</b>
End Position:	74	cm	
Patient Sex:	m		<b>6</b>
<b>Acquisition Parameters:</b>			
Tube current	200	mA	<b>7</b>
Rotation time	0.5	s	<b>8</b>
mAs / Rotation	100	mAs	
Collimation	24	mm	<b>9</b>
Slice Width	5	mm	<b>10</b>
Pitch	1		<b>11</b>
Rel. CTDI	Look up	1.11	at selected collimation
CTDI (air)	Look up	17.0	mGy/100mAs
CTDI (soft tissue)		18.2	mGy/100mAs
nCTDI <sub>w</sub>	Look up	6.6	mGy/100mAs

**Figure 3.17** The procedure of calculation.

The procedure of calculation:

1. Select the scanner manufacturer from the drop down list
2. Select the scanner model from the drop down list
3. Select the appropriate scan kV
4. Choose head or body
5. Enter the start and end positions of the scan series or can be taken from the shaded area on the Phantom worksheet diagram. It is shown in figure 3.18. The user can be adjusted using the up and down arrows. Pressing the 'Get From Phantom Diagram' button enters these values into the start and end position boxes in Scan Calculation
6. Enter 'm' or 'f' in this cell for male or female patients. If left blank, the program will use an average value
7. Enter the x-ray tube current
8. Enter the scanner tube rotation time
9. Choose collimation
10. Enter slice width
11. Enter pitch
12. Push the button 'Update Data Set' when the all values are entered then will get the results

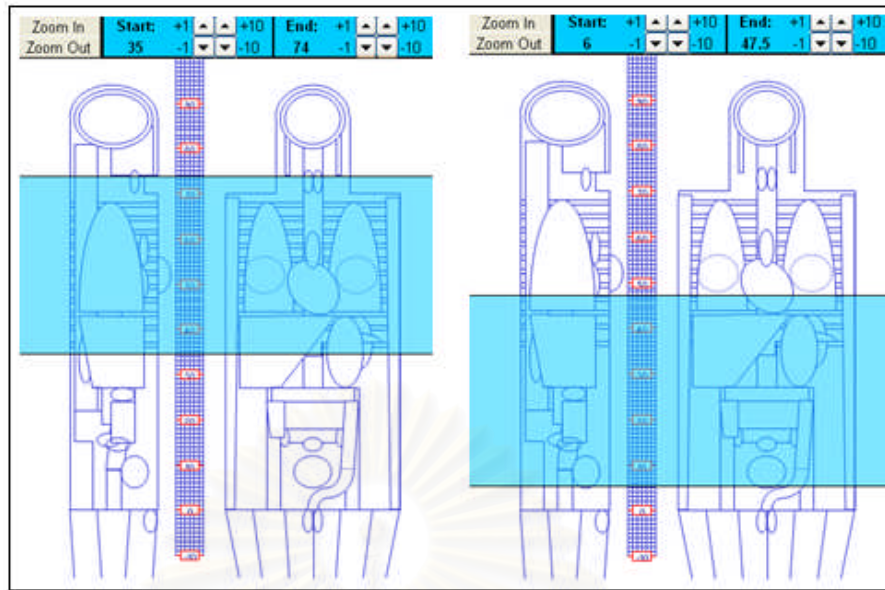


Figure 3.18 Start and end positions of scan range.

### ImpACT CT Patient Dosimetry Calculator

Version 0.99x 20/01/06

<b>Scanner Model:</b>				<b>Acquisition Parameters:</b>			
Manufacturer:	Siemens			Tube current	200	mA	
Scanner:	Siemens Sensation 16			Rotation time	0.5	s	
kV:	120			mAs / Rotation	100	mAs	
Scan Region:	Body			Collimation	24	mm	
Data Set	MCSET23	Update Data Set		Slice Width	5	mm	
Current Data	MCSET23			Pitch	1		
<b>Scan range</b>				Rel. CTDI	Look up	1.11	at selected collimation
Start Position	35	cm	Get From Phantom	CTDI (air)	Look up	17.0	mGy/100mAs
End Position	74	cm	Diagram	CTDI (soft tissue)	18.2	mGy/100mAs	
Patient Sex:	m			$nCTDI_w$	Look up	6.6	mGy/100mAs

Organ	$w_T$	$H_T$	$w_T \cdot H_T$
Gonads	0.2	0.035	0.0071
Bone Marrow (red)	0.12	3.4	0.41
Colon	0.12	0.064	0.0077
Lung	0.12	10	1.2
Stomach	0.12	4.9	0.58
Bladder	0.05	0.021	0.001
Breast	0.05	8.3	0.42
Liver	0.05	6.1	0.31
Oesophagus (Thymus)	0.05	11	0.57
Thyroid	0.05	12	0.6
Skin	0.01	2.7	0.027
Bone Surface	0.01	6.6	0.066
Remainder 1	0.025	2.6	0.065
Remainder 2	0.025	2.6	0.065
<b>Total Effective Dose (mSv)</b>			<b>4.4</b>

Remainder Organs	$H_T$
Adrenals	8
Brain	0.19
Upper Large Intestine	0.37
Small Intestine	0.28
Kidney	2.7
Pancreas	6.4
Spleen	6.2
Thymus	11
Uterus	0.057
Muscle	2.7

$CTDI_w$ (mGy)	6.6
$CDTI_{vol}$ (mGy)	6.6
DLP (mGy.cm)	259

Figure 3.19 The report of calculation.

### 3.7.2 Thermoluminescent dosimetry method

#### 3.7.2.1 Thermoluminescent dosimeter preparation [27]

##### A) Sensitivity and dose calibration

The sensitivity of each dosimeter was determined by exposing 10 cGy of  $^{60}\text{Co}$  (gamma-ray) to 83 dosimeters, the charge integral value of each dosimeter was read and the ECC was calculated according to equation 2.14. The dosimeters that have the ECC values between 0.9 and 1.1 were selected for using in study. The TLDs that were not in this range were removed, leaving of 67 ships. In addition, the dosimeters of the ECC values varied by  $\pm 1\%$  (0.99 to 1.01) were chosen for absorbed dose calibration. The known absorbed dose of 10 cGy of  $^{60}\text{Co}$  (gamma-ray) from ELDORADO 78  $^{60}\text{Co}$  teletherapy were irradiated to these dosimeters, the average value of charge integral reading was used as a factor to convert charge to absorbed dose. This is RCF value. The definition is shown in equation 2.16.

##### B) Linearity

To obtain the linearity of the TLD response, the dosimeters were irradiated in water phantom with  $^{60}\text{Co}$  (1.25 MeV) with the absorbed dose of 20, 50, 70 and 100 mGy. Three dosimeters were loaded in the plastic tube which was inserted in the hole of water phantom at 2 cm depth. 2 tubes with 6 dosimeters were irradiated.

##### C) Energy response

The energy response was determined by measuring the radiation profile. Using 33 TLDs stacked in the z direction of about 10 cm in the body phantom. They are shown in figure 3.20. The technique for scan was 120 kVp, 100 mAs, 10 mm slice width, 10 mm collimation, and 350 mm FOV. The integral response of TLD was obtained by using MATLAB. The absolute doses delivered to these TLDs were determined by measuring the integral dose in the z direction using 10 cm long pencil ionization chamber. It is shown in figure 3.20. Then the energy response relative to cobalt-60 gamma beams was obtained by the ratio of the TLD response for cobalt-60 gamma beams and x-ray beam from CT at the same absolute dose.

สถาบันวิทยบริการ  
จุฬาลงกรณ์มหาวิทยาลัย



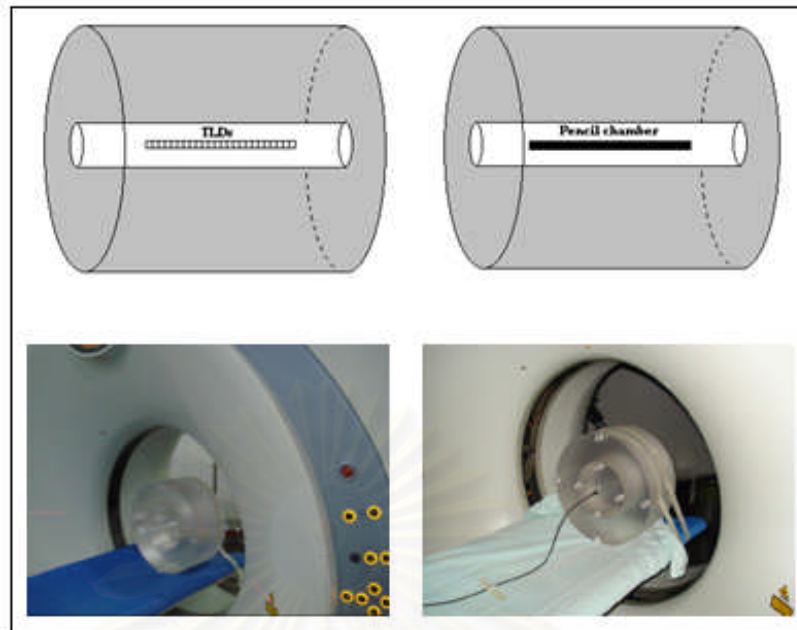


**Figure 3.20** The phantom with thermoluminescent dosimeters for radiation profile measurement.

#### D) Minimum detectable dose

The 18 TLD chips were read for background, for evaluation of the minimum detectable dose (MDD), the coefficient of variation (CV) were determined then the MDD was calculated as:

$$MDD = 3 \times CV \times BG \quad (3.1)$$

#### 3.7.2.2 The thermoluminescent dosimeter positions in Rando phantom

The positions to place the TLDs in each organ of interest were determined and marked in each slice of the phantom. These points were based on a human anatomy CT atlas. The fusion image procedure was used to obtain the corrected positions. They are shown in figure 3.21.

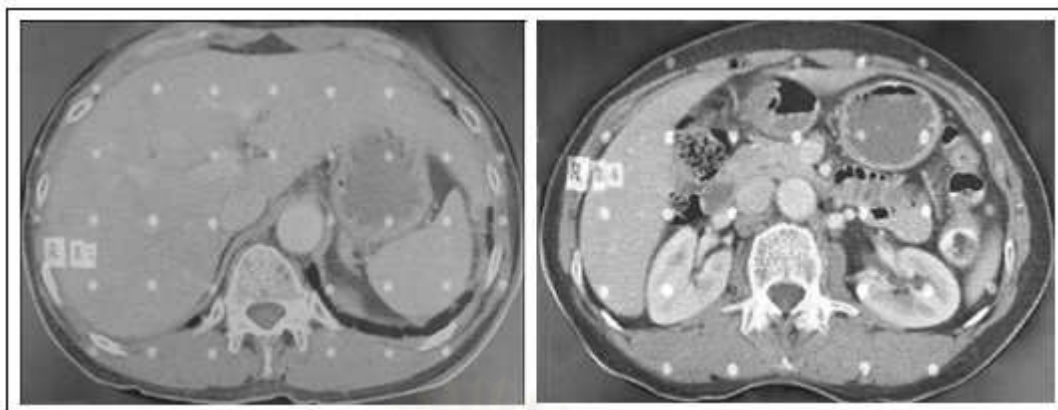


**Figure 3.21** The marked position of some organs in a single slice of the phantom.

### 3.7.2.3 The Rando phantom scanning

The Rando phantom was scanned in chest and abdominal protocols, the exposure parameters used are shown in table 3.1. For a chest examination, the 8<sup>th</sup> slab to 23<sup>rd</sup> slab and an abdominal examination, the 18<sup>th</sup> slab to 34<sup>th</sup> slab of Rando phantom were used. The exposure was repeated 4 times, so a minimum of 12 TLD chips in each organ was recorded.

**Table 3.1** Computed tomography exposure factors and protocols.

Scan	kVp	mAs	Pitch	Slice width (mm)	Collimation (mm)	Scan length (mm)
Chest	120	100	1	5	24	390
Abdomen	120	140	1	8	24	415



**Figure 3.22** The Rando phantom scanning.

### 3.7.2.4 Thermoluminescent dosimeter reading

After the TLDs had been exposed, they were removed from the phantom and were read 24 hr later. They were read in the Harshaw model 5500 automatic TLD reader.



**Figure 3.23** The unit of the automatic thermoluminescent dosimeter reader.

### 3.7.2.5 Converted the effective dose

The reading values were reported to absorbed dose then they were corrected by energy correction factor. Finally the absolute doses were converted to the effective dose as:

$$\text{Effective dose} = \text{organ dose} \times \text{tissue weighting factor} \quad (3.2)$$

## 3.8 Data collection

The ionization chamber measured the CTDI in air and in the PMMA phantom for Monte Carlo method. And after the TLDs have been irradiated, they were read out on the Harshaw model 5500 automatic TLD reader for thermoluminescent dosimetry method.

## 3.9 Data analysis

### 3.9.1 Uncertainty of TLD measurement

The uncertainty budget of TLD measurement with 95% confidence level was calculated.

### 3.9.2 Summarization of data

The effective doses from CT examination were calculated by ImPACT spreadsheet program for Monte Carlo method and by equation 3.2 for thermoluminescent dosimetry method. Finally they were compared for the percentage difference.

### 3.9.3 Data presentation

The table and scatter chart were presented.

### 3.10 Benefit of the study

The actual effective dose for patient undergoing computed tomography examinations for Siemens sensation 16.

### 3.11 Ethic consideration

The measurement was performed in the phantom and the ethical approval by Ethics Committee of Faculty of Medicine, Chulalongkorn University was already processed.



# CHAPTER 4

## RESULTS

### 4.1 Monte Carlo simulation

#### 4.1.1 Measurement of computed tomography dose index

The CTDI in the air and the body phantom for the measurement, calculation and ImPACT are shown in table 4.1. The mean CTDI measured in the air indicated 15.25 mGy and the mean CTDI measured in the body phantom indicated 3.53 mGy at the center and 7.16 mGy at the periphery. The ImPACT values in the phantom showed higher values than the measured, the difference for CTDI<sub>w</sub> between measured and ImPACT was 12.88% while the difference between measured and calculated by manufactured was 5.56%.

**Table 4.1** Computed tomography dose index in the air and the body phantom.

CTDI	Mean measured value (mGy/100 mAs)	Calculated value (mGy/100 mAs)	ImPACT value (mGy/100 mAs)
In air	15.25	-	15.26
Center	3.53	-	4.17
Periphery	7.16	-	8.16
CTDI <sub>w</sub>	5.95	6.30	6.83

#### 4.1.2 The organ doses and effective doses from Monte Carlo simulation

##### 4.1.2.1 Chest examination

The organ doses, tissue doses and the effective doses together with the tissue weighting factors used for calculation by ImPACT program of Monte Carlo simulation for chest examination are shown in table 4.2. The organ doses outside the irradiated field that were bladder, gonads and colon demonstrated the low dose range from 0.02 to 0.07 mGy, while organs and tissues that were in the chest irradiated field showed the higher dose ranged from 2.28 to 12.00 mGy. When the effective doses were calculated using tissue weighting factors published in ICRP 60 [11], the effective dose was 4.37 mSv.

**Table 4.2** The organ doses, tissue doses and effective doses of chest examination by Monte Carlo simulation.

Organ	Organ and tissue doses (mGy)	Tissue weighting factor	Effective dose (mSv)
Gonads	0.055	0.20	0.011
Bone marrow (red)	3.417	0.12	0.410
Colon	0.067	0.12	0.008
Lung	10.000	0.12	1.200
Stomach	5.000	0.12	0.600
Bladder	0.020	0.05	0.001
Breast	8.400	0.05	0.420
Liver	6.200	0.05	0.310
Esophagus	12.000	0.05	0.600
Thyroid	12.000	0.05	0.600
Skin	3.000	0.01	0.030
Bone surface	6.600	0.01	0.066
Remainder*	2.280	0.05	0.114
<b>Total</b>			<b>4.370</b>

(Technique: 120 kVp, 100 mAs, 1 pitch, 5 mm slice width, 24 mm collimation, and 390 mm scan length)

\* Adrenals, brain, upper large intestine, small intestine, kidney, pancreas, spleen, thymus, uterus, and muscle

#### 4.1.2.2 Abdominal examination

The organ doses, tissue doses and the effective doses together with tissue weighting factors used for calculation by Monte Carlo simulation for abdominal examination are also shown in table 4.3. The organ doses outside the irradiated field that were thyroid, esophagus and breast demonstrated the low dose range from 0.06 to 0.86 mGy, while organs and tissues that were in the abdominal irradiated field showed the higher dose range from 3.70 to 14.00 mGy. These organ doses and tissue doses made the effective of 7.31 mSv.

**Table 4.3** The organ doses, tissue doses and effective doses of abdominal examination by Monte Carlo simulation.

Organ	Organ and tissue doses (mGy)	Tissue weighting factor	Effective dose (mSv)
Gonads	9.000	0.20	1.800
Bone marrow (red)	5.333	0.12	0.640
Colon	8.167	0.12	0.980
Lung	4.250	0.12	0.510
Stomach	13.333	0.12	1.600
Bladder	10.000	0.05	0.500
Breast	0.860	0.05	0.043
Liver	12.400	0.05	0.620
Esophagus	0.760	0.05	0.038
Thyroid	0.060	0.05	0.003
Skin	3.700	0.01	0.037
Bone surface	7.000	0.01	0.070
Kidneys	14.000	0.025	0.350
Remainder**	4.800	0.025	0.120
<b>Total</b>			<b>7.311</b>

(Technique: 120 kVp, 140 mAs, 1 pitch, 8 mm slice width, 24 mm collimation, and 415 mm scan length)

\*\* Adrenals, brain, upper large intestine, small intestine, pancreas, spleen, thymus, uterus, and muscle

## 4.2 Thermoluminescent dosimetry

### 4.2.1 Thermoluminescent dosimeter characteristics

#### 4.2.1.1 Sensitivity

The sensitivity or the element correction coefficient factors (ECC) of individual TLD chip was sorted by its readout from the same dosage of 10 cGy. The sensitivity of each TLD was normalized to the average sensitivity to get the sensitivity factors for each TLD according to equation 2.14. The element correction coefficient factors ranged from 0.9001 to 1.0837 for the TLD chips that were used in this study. They are shown in table 4.4. Eleven TLDs which had the sensitivity factors ranging from 0.9930 to 1.0075 were selected to be used in the calibration of RCF by equation 2.16, they are shown in table 4.5. The RCF was  $2.962 \times 10^{-5}$  nC/cGy.

**Table 4.4** The sensitivity correction values of 67 thermoluminescent dosimeter chips that were used for measurement.

Number	ECC	Number	ECC	Number	ECC
1	0.9894	24	0.9361	47	1.0589
2	1.0215	25	0.9309	48	1.0631
3	1.0490	26	0.9475	49	1.0292
4	1.0301	27	0.9338	50	1.0541
5	0.9562	28	0.9525	51	1.0716
6	1.0649	29	0.9412	52	1.0796
7	1.0555	30	0.9797	53	1.0703
8	1.0437	31	0.9478	54	1.0551
9	1.0324	32	0.9603	55	1.0607
10	0.9001	33	0.9689	56	1.0739
11	0.9164	34	0.9496	57	1.0443
12	0.9452	35	1.0306	58	1.0413
13	0.9547	36	0.9786	59	1.0048
14	0.9270	37	0.9683	60	1.0128
15	0.9276	38	1.0111	61	1.0837
16	0.9479	39	1.0735	62	1.0723
17	1.0339	40	0.9869	63	1.0140
18	1.0128	41	1.0535	64	1.0395
19	0.9406	42	0.9971	65	1.0222
20	0.9381	43	0.9778	66	1.0439
21	0.9382	44	0.9501	67	0.9878
22	0.9596	45	0.9636		
23	0.9147	46	1.0777	SD	5.28

*ECC = The element correction coefficient*

**Table 4.5** The sensitivity correction values of 11 thermoluminescent dosimeter chips that were used for calibration.

Number	ECC	Number	ECC
1	0.9930	7	1.0038
2	1.0071	8	0.9971
3	1.0075	9	1.0044
4	0.9937	10	0.9966
5	1.0014	11	0.9930
6	1.0026	SD = 2.00	



## 4.2.1.2 Linearity

The charges corrected by the various doses from 20 to 100 mGy for  $^{60}\text{Co}$  (1.25 MeV) were shown in table 4.6 and figure 4.1. The graph showed the linear relationship between TLDs and absorbed dose responses with the correlation coefficient of 0.999.

**Table 4.6** The absorbed doses in  $^{60}\text{Co}$  and reading value of thermoluminescent dosimeter responses.

Number	Absorbed dose in $^{60}\text{Co}$ (mGy)	Reading value of TLDs (nC)	
		Mean	SD
1	20	55.21	0.53
2	50	155.79	2.32
3	70	208.96	2.71
4	100	306.78	4.66

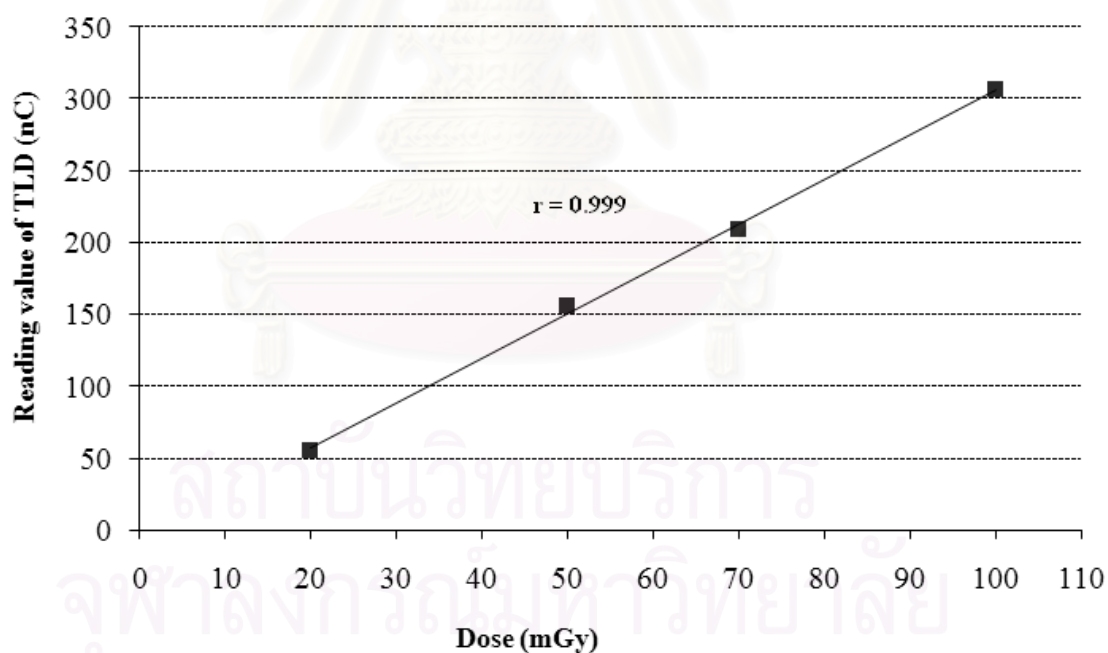


**Figure 4.1** The relation between thermoluminescent dosimeters and absorbed doses.

#### 4.2.1.3 Energy response

The energy response of the TLDs in CT x-ray beam related to cobalt-60 gamma rays were obtained by using the method of the integral value of TLD response in a radiation profile equal to the CTDI dose measured by pencil ionization chamber, the data for radiation profile are shown in table 4.7, the profile was plotted for raw data, it is shown in figure 4.2, and the MATLAB calculation for the radiation profile was also investigated, it is shown in figure 4.3. Then area of the curve was processed by MATLAB to get the TLD response value. The energy correction factor of x-ray beam from CT related to cobalt-60 at the absorbed dose of 50 mGy was calculated by equation 4.1, which was 0.6.

$$\text{The correction factor} = \text{reading value from cobalt-60} / \text{reading value from CT} \quad (4.1)$$

**Table 4.7** Reading values of thermoluminescent dosimeters for radiation profile.

Position (mm)	Reading value (nC)	Position (mm)	Reading value (nC)	Position (mm)	Reading value (nC)
-51.2	1.216	-16.0	1.775	19.2	1.779
-48.0	1.086	-12.8	1.895	22.4	1.752
-44.8	1.116	-9.6	1.940	25.6	1.648
-41.6	1.127	-6.4	2.180	28.8	1.485
-38.4	1.296	-3.2	3.570	32.0	1.434
-35.2	1.280	0	3.559	35.2	1.403
-32.0	1.355	3.2	3.680	38.4	1.237
-28.8	1.418	6.4	2.395	41.6	1.234
-25.6	1.529	9.6	2.005	44.8	1.148
-22.4	1.649	12.8	1.943	48.0	1.092
-19.2	1.672	16.0	1.819	51.2	1.022

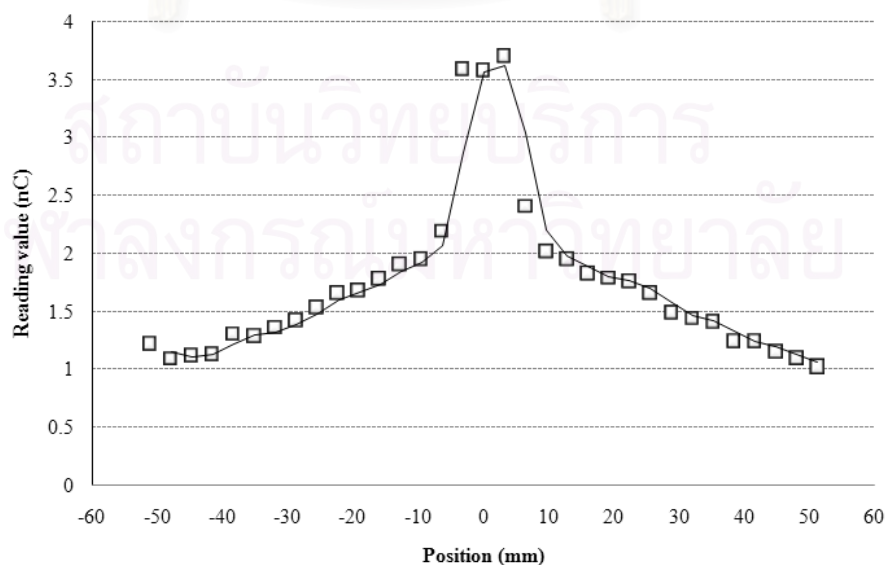


**Figure 4.2** Manual plotted of radiation profile of 10 mm slice thickness.

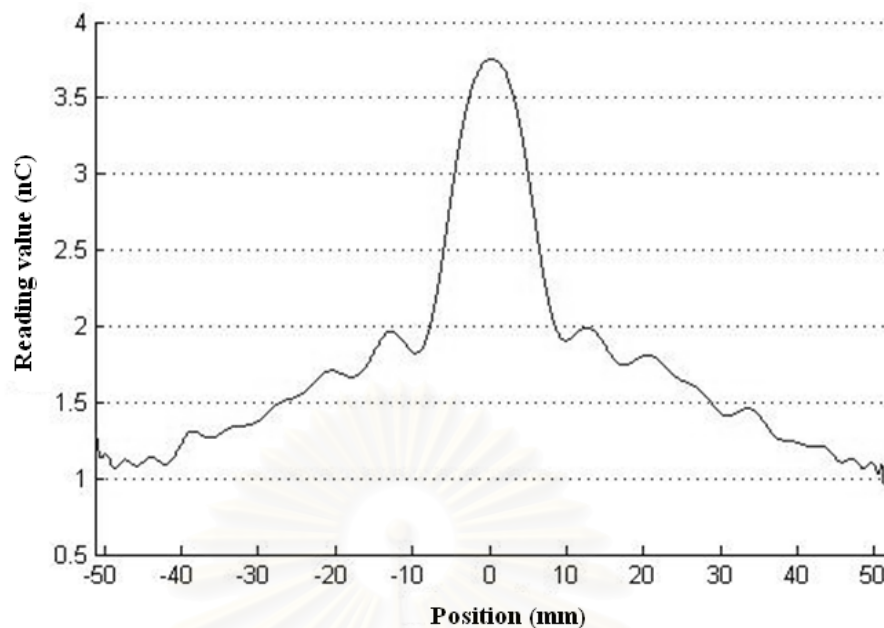


**Figure 4.3** MATLAB plotted of radiation profile of 10 mm slice thickness.

#### 4.2.1.4 Minimum detectable dose

The data for calculation of minimum detectable dose are shown in table 4.8. The calculated value by equation 3.1 was 0.029 mGy.

**Table 4.8** Reading values of background.

Number	Reading values (mGy)	Number	Reading values (mGy)
1	0.036	12	0.038
2	0.054	13	0.023
3	0.057	14	0.030
4	0.048	15	0.028
5	0.032	16	0.032
6	0.050	17	0.029
7	0.038	18	0.035
8	0.034	<b>Mean</b>	<b>0.0375</b>
9	0.032	<b>SD</b>	<b>0.0096</b>
10	0.047	<b>CV</b>	<b>0.2571</b>
11	0.032		

## 4.2.2 Uncertainty of TLD measurement [28]

The uncertainty of TLD measurement is shown in table 4.9 and steps of determination of the uncertainty are shown in appendix C.

**Table 4.9** Uncertainty budgets and the expanded uncertainty of dose measurement using TLD measurement in Rando phantom.

Sources of uncertainty	Value* (%)	Probability distribution	Divisor	Uncertainty (%)
1. TLD sensitivity	5.28	Normal	1	5.28
2. TLD calibration				
- TLDs	1.15	Normal	1	1.15
- Ionization chamber	0.17	Normal	1	0.17
3. Calibration factor of ionization chamber (calibration certificate)	0.60	Normal	2	0.3
4. Measuring accuracy	1.83	Normal	1	1.83
Combined uncertainty				5.72
Expanded uncertainty (k=2), 95% confidence level				11.74

\*Standard uncertainty

## 4.2.3 The organ doses and effective doses from thermoluminescent dosimetry

## 4.2.3.1 Chest examination

The organ doses, tissue doses and the effective doses together with tissue weighting factors used for calculation by TLD measurement for chest examination are shown in table 4.10. The results were agreeable with the Monte Carlo simulation. The organ doses and tissue doses outside the irradiated field that were bladder, gonad and colon demonstrated the low dose, they ranged from 0.13 to 1.56 mGy, while organs and tissues that were in the irradiated field showed the higher dose, they ranged from 3.41 to 12.13 mGy. These organ doses made the effective dose of 5.416 mSv.

**Table 4.10** The organ doses, tissue doses and effective doses of thermoluminescent dosimetry for chest examination.

Organ	Mean organ and tissue doses (mGy)	SD	Tissue weighting factor	Effective dose (mSv)
Gonads	0.135	0.02	0.20	0.027
Bone marrow (red)	5.278	0.34	0.12	0.633
Colon	1.563	0.06	0.12	0.188
Lung	11.111	0.48	0.12	1.333
Stomach	7.056	0.25	0.12	0.847
Bladder	0.227	0.02	0.05	0.011
Breast	8.267	0.23	0.05	0.413
Liver	10.000	0.53	0.05	0.500
Esophagus	11.267	0.12	0.05	0.563
Thyroid	12.133	0.12	0.05	0.607
Skin	6.100	0.78	0.01	0.061
Bone surface	6.233	0.06	0.01	0.062
Remainder*	3.412	0.05	0.05	0.171
<b>Total</b>				<b>5.416</b>

(Technique: 120 kVp, 100 mAs, 1 pitch, 5 mm slice width, 24 mm collimation, and 390 mm scan length)

\* Adrenals, brain, upper large intestine, small intestine, kidney, pancreas, spleen, thymus, uterus, and muscle

#### 4.2.3.2 Abdominal examination

The organ doses, tissue doses and the effective doses together with tissue weighting factors used for calculation by TLD measurement for abdominal examination are also shown in table 4.11. Again the results were agreeable with the Monte Carlo simulation. The organ and tissue doses outside the irradiated field that were thyroid, esophagus and breast demonstrated the low dose range from 0.22 to 1.35 mGy, while organs and tissues that were in the irradiated field showed the higher dose range from 4.00 to 16.40 mGy. These organ doses made the effective of 8.523 mSv.

**Table 4.11** The organ doses, tissue doses and effective doses of thermoluminescent dosimetry for abdominal examination.

Organ	Mean organ and tissue doses (mGy)	SD	Tissue weighting factor	Effective dose (mSv)
Gonads	7.456	0.17	0.20	1.491
Bone marrow (red)	8.233	0.28	0.12	0.988
Colon	13.694	0.46	0.12	1.643
Lung	4.000	0.08	0.12	0.480
Stomach	14.411	0.23	0.12	1.729
Bladder	13.467	0.61	0.05	0.673
Breast	1.347	0.02	0.05	0.067
Liver	14.200	0.42	0.05	0.710
Esophagus	0.445	0.45	0.05	0.022
Thyroid	0.227	0.05	0.05	0.011
Skin	6.600	1.00	0.01	0.066
Bone surface	8.233	0.38	0.01	0.082
Kidneys	16.400	0.40	0.025	0.410
Remainder**	6.047	0.14	0.025	0.151
<b>Total</b>				<b>8.523</b>

(Technique: 120 kVp, 140 mAs, 1 pitch, 8 mm slice width, 24 mm collimation, and 415 mm scan length)

\*\* Adrenals, brain, upper large intestine, small intestine, pancreas, spleen, thymus, uterus, and muscle

The standard deviation for organ and tissue doses for both chest and abdominal examinations showed small number. The large value of standard deviation indicated the variation of doses due to the difference of location of TLDs between the measurements.

### 4.3 Comparison of the organ doses and effective doses between two methods

#### 4.3.1 Chest examination

The comparison of the organ doses and effective doses of Monte Carlo simulation and thermoluminescent dosimetry for chest examination are shown in table 4.12. The correlation of the organ doses from thermoluminescent dosimetry and Monte Carlo simulation of chest examination is shown in figure 4.4. The solid line of the graph represented the value of equal organ doses between TLD dose measurement and Monte Carlo simulation, the organ doses were plotted between the value of Monte Carlo simulation and the value of TLD dose measurement with the data of 11.74% uncertainties. The measured gonads, colon, and bladder which were the organs outside the irradiated area gave the small dose of less than 1.6 mGy. They showed the large percentage difference between two methods of up to 95.71%. The organs that situated near the edge of the beam demonstrated the difference of 38.00% for liver and 29.14% for stomach. The bone marrow (red) and skin that were difficult to search for the exact location as the MIRD mathematical phantom in Monte Carlo simulation, showed the difference of 35.26% and 50.82%, respectively. Other than the mentioned criteria, the organ doses between calculated and measured seem to be agreed within 11.74% uncertainty. The total effective doses were 4.37 mSv for calculation and 5.42 mSv for measurement with the difference of 19.37%.

**Table 4.12** Comparison of the organ doses and effective doses between thermoluminescent dosimetry and Monte Carlo simulation for chest examination.

Organ	Thermoluminescent dosimetry (mGy)	Monte Carlo simulation (mGy)	Percentage difference
Gonads	0.135	0.055	59.26
Bone marrow (red)	5.278	3.417	35.26
Colon	1.563	0.067	95.71
Lung	11.111	10.000	10.00
Stomach	7.056	5.000	29.14
Bladder	0.227	0.020	90.91
Breast	8.267	8.400	- 1.61
Liver	10.000	6.200	38.00
Esophagus	11.267	12.000	- 6.51
Thyroid	12.133	12.000	1.10
Skin	6.100	3.000	50.82
Bone surface	6.233	6.600	- 5.89
Remainder	3.412	2.280	33.18
<b>Effective dose (mSv)</b>	<b>5.42</b>	<b>4.37</b>	<b>19.37</b>

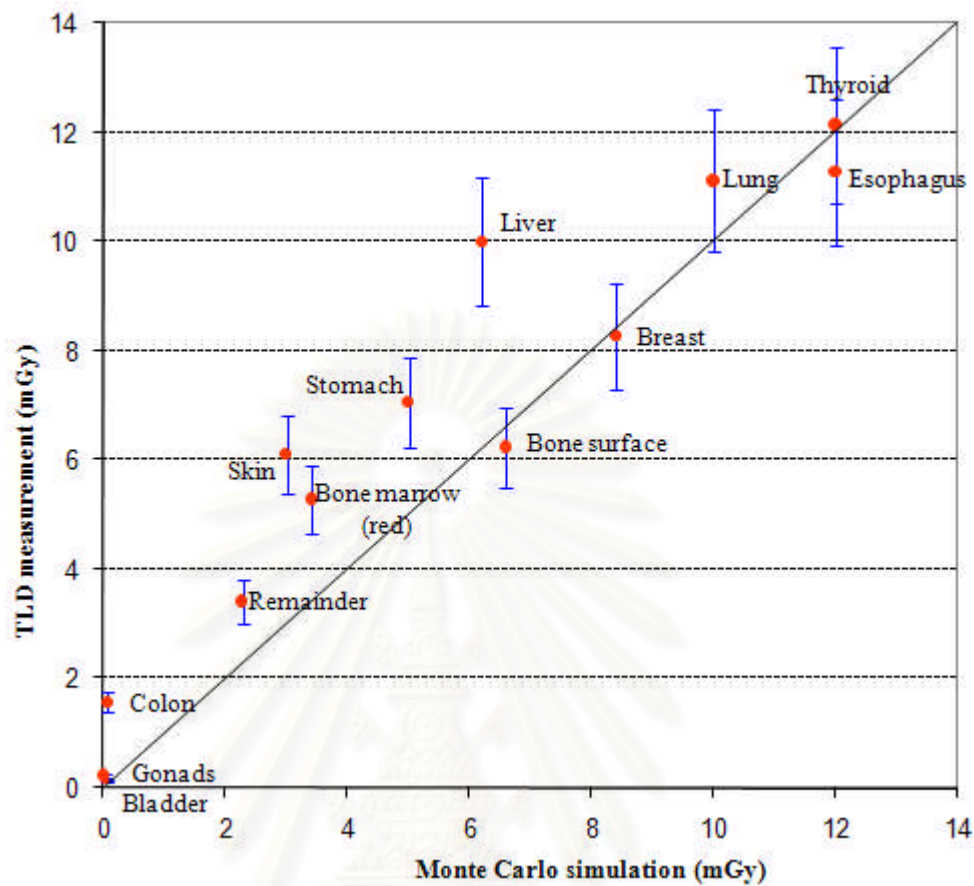


**Figure 4.4** The correlation of the organ doses from thermoluminescent dosimetry with 11.74% uncertainty of TLD measurement and Monte Carlo simulation of chest examination.



### 4.3.2 Abdominal examination

The comparison of the organ doses and effective doses of Monte Carlo simulation and thermoluminescent dosimetry for abdominal examination are shown in table 4.13. The correlation of the organ doses from thermoluminescent dosimetry and Monte Carlo simulation of abdominal examination is shown in figure 4.5. The solid line of the graph represented the value of equal organ doses between TLD dose measurement and Monte Carlo simulation, the organ doses were plotted between the value of Monte Carlo simulation and the value of TLD dose measurement with the data of 11.74% uncertainties. Again the thyroid and esophagus which were the organs outside the irradiated area showed the large percentage difference up to 73.57%. However, the small organ dose of less than 0.5 mGy made the difference became large. The organs that situated near the edge of the beam demonstrated the difference of 36.15% for breast. Again the bone marrow (red), skin, colon, and bladder that were difficult to search for the exact location showed the large difference of 35.22%, 43.94%, 40.36%, and 25.74%, respectively. Other than the mentioned criteria, the organ doses between calculated and measured seem to be agreed within 11.74% uncertainty. The effective doses were 7.31 mSv for calculated and 8.52 mSv for measurement with the total effective dose difference of 14.20%.

**Table 4.13** Comparison of the organ doses and effective doses between thermoluminescent dosimetry and Monte Carlo simulation for abdominal examination.

Organ	Thermoluminescent dosimetry (mGy)	Monte Carlo simulation (mGy)	Percentage difference
Gonads	7.456	9.000	- 20.71
Bone marrow (red)	8.233	5.333	35.22
Colon	13.694	8.167	40.36
Lung	4.000	4.250	- 6.25
Stomach	14.411	13.333	7.48
Bladder	13.467	10.000	25.74
Breast	1.347	0.860	36.15
Liver	14.200	12.400	12.68
Esophagus	0.445	0.760	- 70.79
Thyroid	0.227	0.060	73.57
Skin	6.600	3.700	43.94
Bone surface	8.233	7.000	14.98
Kidneys	16.400	14.000	14.63
Remainder*	6.047	4.800	20.62
<b>Effective dose (mSv)</b>	<b>8.52</b>	<b>7.31</b>	<b>14.20</b>

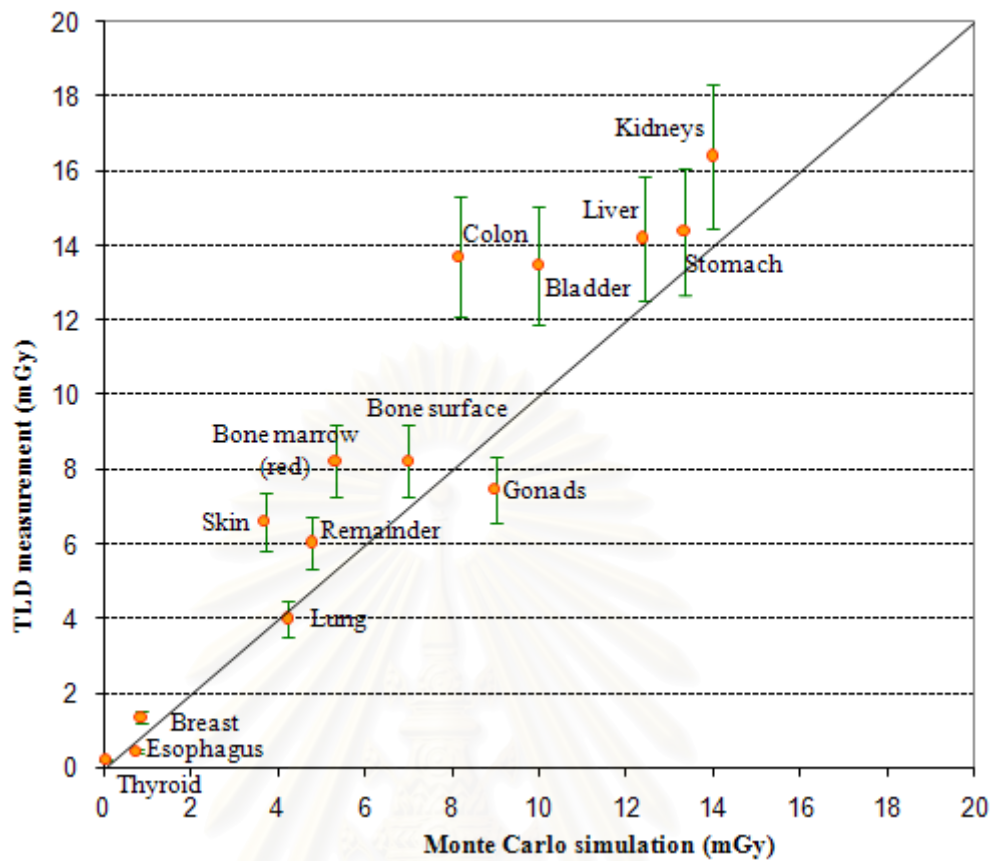


**Figure 4.5** The correlation of the effective doses from thermoluminescent dosimetry with 11.74% uncertainty of TLD measurement and Monte Carlo simulation of abdominal examination.

สถาบันวิทยบริการ  
จุฬาลงกรณ์มหาวิทยาลัย

# CHAPTER 5

## DISCUSSION AND CONCLUSION

### 5.1 Discussion

The advent of computed tomography has revolutionized diagnostic radiology since the inception of CT in the 1970s, its use has increased rapidly. CT involves larger radiation doses than the more common, conventional x-ray imaging procedures. Although the consequent cancer risks for any one person are not large, the increasing exposure to radiation in the population may be a public health issue in the future. The development of techniques leading to estimate either by measuring or calculating of the doses associated with the CT practice has evolved in parallel with its clinical used. Thus, the methodology to estimate the organ and effective dose from CT examination by the calculation and measurement are very important.

5.1.1 The comparison of computed tomography dose index from measured, calculated, and ImpACT values

The CTDI in air agreed well with the ImpACT value but difference for measurement in phantom. The calculated effective dose by Monte Carlo simulation depended on the CTDI value. The measured CTDI<sub>w</sub> was lower than the ImpACT and the calculated values, these would make the less of effective dose calculated by Monte Carlo simulation.

5.1.2 The uncertainty of thermoluminescent dosimeters

The uncertainty of TLDs used in this study was  $\pm 11.74\%$  for 95% confidence level, the minimum dose that TLDs could be measured was 0.029 mGy so the dose lower than this amount could not be detected correctly. The Monte Carlo simulation showed the bladder dose of 0.02 mGy which was lower than the minimum detectable of TLDs. This made the dose uncertainty. Also the lower doses outside irradiation field would give the dose uncertainty due to the low sensitivity of TLD at the low doses.

5.1.3 Comparison of the organ doses and effective doses between Monte Carlo simulation and thermoluminescent dosimetry

5.1.3.1 The organ doses

From our study, most of the organ doses for chest and abdominal examinations from thermoluminescent dosimetry were higher than those calculated by Monte Carlo simulation except breast, esophagus, and bone surfaces for chest examination and gonads, lung, and esophagus for abdominal examination. The differences between the organ doses from two methods were within 11.74% uncertainty of TLD measurement for the organ located in the radiation field except the organs that were difficult to search for the exact location.

The underestimation by Monte Carlo simulation for our study has also been noted by other studies [19 - 20, 22]. The suggested underestimation by Monte Carlo

technique has been attributed to design differences between the Rando phantom and MIRD mathematical phantom and also the accurate employment of normalized organ doses [20, 22]. The computer simulated technique employs the mathematical MIRD phantom, which approximates the organs by simplified geometric shapes, contrary to the situation in practical circumstances. The Rando phantom is a different size compared with the mathematical phantom and the estimated location of the organs in the Rando phantom as used in our study differed significantly in comparison with the distribution of organs in the mathematical phantom. In the mathematical phantom there is a sharp boundary between the thoracic organs and the organ of the abdomen where as in the Rando phantom a more realistic distribution of organs was chosen such as the important part of liver and stomach was located between the lower parts of the lung. So our measurement results for a chest examination yield therefore relatively higher dose in liver and stomach which the important part were in the radiation field, and the more difference of dose between calculated and measured were observed.

There is a difference between the male and female doses. This is due to the more superficial anatomical location of the male gonad in the scrotum, rather than the deeper placement of the ovaries in the pelvis. As a consequence the female gonad exposure is less. The gonad doses in our study were the average between man and woman.

#### 5.1.3.2 The effective doses

The effective doses of this study compared with other studies are shown in table 4.14 and table 4.15 for chest and abdominal examinations, respectively.

**Table 5.1** Comparison of effective doses with the other studies for chest examination.

	This study		Geleijns J [20]		Hashemi MB [22]	
	TLD	MC*	TLD	MC	TLD	MC
CT scanner	Siemens		Philips		Philips	
Model	Sensation 16		LX		Tomoscan CX/S	
Detector	Multi detector		Single slice		Single slice	
mAs	100		380			
kVp	120		120			
Effective dose (mSv)	5.42	4.37	18.00	11.00	9.74	8.10
Percentage difference	19.37%		38.89%		16.84%	

\*Monte Carlo simulation

**Table 5.2** Comparison of effective doses with the other studies for abdominal examination.

	This study		Geleijns J [20]		Hashemi MB[22]	
	TLD	MC	TLD	MC	TLD	MC
CT scanner	Siemens		Philips		Philips	
Model	Sensation 16		LX		Tomoscan CX/S	
Detector	Multi detector		Single slice		Single slice	
mAs	140		333			
kVp	120		120			
Effective dose (mSv)	8.52	7.31	24.00	15.00	17.89	12.30
Percentage difference	14.20%		37.50%		31.25%	

The effective dose in this study for chest examination from Monte Carlo simulation was 4.37 mSv which was lower than the measurement of 5.42 mSv, the difference was 19.37%. The result showed lower dose difference than the previous work of Geleijns J et al [20] who reported the effective dose for chest examination of the measurement of 18 mSv compared with 11 mSv for Monte Carlo simulation. Their result showed about 38.89% dose difference. Their effective dose was rather higher value than our effective dose because they used differences CT protocols and also the CT was the type of single slice. The other study of Hashemi MB et al [22] obtained the lower difference than our study. The effective doses were 9.74 mSv for the measurement and 8.10 mSv for Monte Carlo simulation resulting in 16.84% difference.

The effective doses in this study for abdominal examination from Monte Carlo simulation were 7.31 mSv and 8.52 mSv for thermoluminescent dosimetry. The difference was 14.20%. The result showed lower dose difference than the previous work of Geleijns J et al [20] who showed the effective dose for abdominal examination of the measurement of 24 mSv compared to 15 mSv for Monte Carlo simulation. Their result showed about 37.50% dose difference. While the study of Hashemi MB et al [22] reported the effective dose of 17.89 mSv for the measurement and 12.3 mSv for Monte Carlo simulation resulting in 31.25% difference. The difference was comparable to Geleijns J.

Groves AM et al [19] measured the effective dose from a 16-detector multi slice for whole body study using TLDs in Rando phantom. They found that the measured was 15.32% higher than the Monte Carlo simulation. The result was also underestimation by computer simulation compared with TLD measurements. Their CT machine was a helical type of Siemens Somatom Sensation16 which was the same type of machine used in our study. The average for both chest and abdominal examination of 16.72% dose difference between calculated and measured were obtained for our study which was comparable to them.

## 5.2 Conclusion

The number of CT examination in Thailand is rapidly growing as it is in other countries. It is important to know the method to estimate the effective dose. Absorbed doses in organs and tissues were obtained from two methods. Direct measurements in

relevant organs were performed with thermoluminescent dosimeters employing a Rando phantom. The other method was based upon the measurement of CTDI with CT ionization chamber. The organ doses and tissue doses would be estimated by Monte Carlo methods and mathematical phantoms. Effective doses were calculated from organ and tissue doses using tissue weighting factors.

The result of the study of the effective doses for a helical type of Siemens Sensation 16 demonstrated that the direct TLD measurements were higher than those of the Monte Carlo technique. The result agreed with the other studies [19 - 20, 22]. The underestimation and the difference between the two dosimetry techniques can be concluded as follows:

1. The design between the Rando phantom and MIRD mathematical phantom may be differences.
2. The Monte Carlo simulated the CT unit to specific model of CT unit that may differ from CT studied unit.
3. The measured CTDI are relatively difference from ImPACT value.
4. The uncertainty of TLDs for each measurement.

However, with the attention of the TLD measurement, direct TLD CT dose estimation has some advantage over computer simulated dosimetry techniques. For the patient under CT examination, the dose estimations can be made by simulations with the awareness of the underestimation.

## REFERENCES

1. Shrimpton PC, Hart D, Hillier MC, Wall BF, Faulkner K. Survey of CT practice in the UK. Part 1: Aspects of examination frequency and quality assurance. Chilton, NRPB-R248 (London, HMSO). 1991.
2. Shrimpton PC, Jones DG, Hillier MC, Wall BF, Le Heron JC, Faulkner K. Survey of CT practice in the UK. Part 2: Dosimetric aspects. Chilton, NRPB-R249 (London, HMSO). 1991.
3. Jones DG, Shrimpton PC. Survey of CT practice in the UK. Part 3: normalized organ doses calculated using Monte Carlo techniques. Chilton, NRPB-R250 (London, HMSO), 1991.
4. Snyder WS, Ford MR, Warner GG, Fhiser HL. Estimates of absorbed fractions for monoenergetic photon sources uniformly distributed in various organs of a heterogeneous phantom. J Nucl Med 10 (Suppl.3), Pamphlet No.5, 1969.
5. Jerrold TB. The essential physics of medical imaging. 2<sup>nd</sup> ed. USA, 2002; 255 – 83, 326 – 72.
6. McNitt-Gray MF. Radiation dose in CT. AAPM/RSNA Physics Tutorial for Residents: Topic in CT. Radio Graphics. 2002; 1541-53.
7. European Guidelines on Quality Criteria for Computed Tomography (EUR 16262 EN, May 1999). Available from: [www.drs.dk/guidelines/ct/quality/index.htm](http://www.drs.dk/guidelines/ct/quality/index.htm).
8. Khan FM. The physics of Radiation Therapy. 3<sup>rd</sup> ed. USA: Lippincott Williams & Wilkins, 2003.
9. Cameron JR, Suntharalingam N, Kenney GN. Thermoluminescent dosimetry. Milwaukee. The University of Wisconsin Press, 1968.
10. Harshaw Bicron radiation measurement produced. Model 5500 automatic TLD reader user's manual Ohio: Saint-Gobian / Norton industrial ceramics, 1993.
11. ICRP. 1990 Recommendations of the International Commission on Radiological Protection. Publication 60, Annals of the ICRP 1991; 21. Oxford, England: Pergamon, 1991.
12. Shrimpton PC, Jones DG. Normalised organ doses for x-ray computed tomography calculated using Monte Carlo techniques and a mathematical anthropomorphic phantom. Radiat Prot Dosimetry 1993; 49: 241-3.
13. Cristy M. Mathematical phantoms representing children of various ages for use in estimates of internal dose. NUREG/CR - 1159 ORNL/NUREG/TM - 367. Oak Ridge, Tenn: Oak Ridge National Laboratory, 1980.
14. Jones DG, Shrimpton PC. Normalised organ doses for x-ray computed tomography calculated using Monte Carlo techniques. NRPB SR-250. Chilton, England: National Radiological Protection Board, 1992.
15. Imaging Performance Assessment of CT (ImPACT) CT patient Dosimetry Calculator, version 0.99m. Created 07/01/2002. Available from: <http://www.impactscan.org/ctdosimetry.htm>

16. Shrimpton PC, Jones DG, Hillier MC, Wall BF, Le Heron JC, Faulkner K. Survey of CT Practice in the UK. Part 2: Dosimetric Aspects, NRPB-R249. London: HMSO, 1991.
17. Le Heron JC. CTDOSE: A User's Guide. Ministry of Health, Christchurch, New Zealand, 1993.
18. Shrimpton PC, Edyvean S. Commentary: CT scanner dosimetry. BJR 1998; 71: 1-3.
19. Groves AM, Owen KE, Courtney HM, Yates SJ, Goldstone KE, Black GM, et al. 16-detector multislice CT: dosimetry estimation by TLD measurement compared with Monte Carlo simulation. BrJ Radiol 2004; 77 (920): 662 – 5.
20. Geleijns J, Van Unnik JG, Zoetelief J, Zweers D, Broerse JJ. Comparison of two methods for assessing patient dose from computed tomography. Br J Radiol 1994; 67: 360 – 5.
21. Janeczek J, Pernicka F. The measurement of CT scanner radiation dose profile using TL dosimeters. Radiation Protection Dosimetry 1995; 60: 231-5.
22. Hashemi-Malayeri B, Williams JR. A practical approach for the assessment of patient doses from CT examinations. Western general Hospital, Edinburgh, 2003. Available from: [www.dundee.ac.uk/medphys/documents/hashemi.pdf](http://www.dundee.ac.uk/medphys/documents/hashemi.pdf).
23. Scanditronix Wellhofer. Calibration protocol for chamber DCT10-RS manual.
24. ImPACT CT Patient Dosimetry Calculator version 0.99q. ImPACT. Medical Devices Agency. London. 2003.
25. International Commission on Radiation Units and Measurements. Tissue substitutes in radiation dosimetry and measurement. Report No.44. Bethesda, MD: International Commission on Radiation Units and Measurements, 1989.
26. Shrimpton PC. Electron density values of various human tissue: in vitro Compton scatter measurements and calculated ranges. Phys Med Biol 1981; 26: 907.
27. International Atomic Energy Agency, Report of a coordinated research programme jointly organized by the International Atomic Energy Agency and the Commission of the European Communities, Radiation doses in Diagnostic Radiology and Methods for Dose Reduction, April 1995: 11-8.
28. United Kingdom Accreditation service. The expression of uncertainty and confidence in measurement. 2<sup>nd</sup> ed. M3003, 2007. Available from: [www.ukas.com](http://www.ukas.com)





**APPENDICES**

สถาบันวิทยบริการ  
จุฬาลงกรณ์มหาวิทยาลัย

## APPENDIX A

### CASE RECORD FORMS

**Table I** Case record form of Monte Carlo simulation.

	Reading value (mGy/100 mAs)				
	No.1	No.2	No.3	No.4	Average
CTDI in air					
CTDI at center of body phantom					
CTDI at periphery of body phantom					

*Technique: 120 kVp, 100 mAs, slice width 10 mm, 2 x 5.0 mm collimation, and 350 mm FOV*

**Table II** Case record form of thermoluminescent dosimetry for chest examination.

“Chest examination” Organ	Reading value (mGy)					
	No.1	No.2	No.3	No.4	Average	SD
Gonads						
Bone marrow (red)						
Colon						
Lung						
Stomach						
Bladder						
Breast						
Liver						
Esophagus						
Thyroid						
Skin						
Bone surface						
Adrenals						
Brain						
Upper large intestine						
Small intestine						
Kidney						
Pancreas						
Spleen						
Thymus						
Uterus						
Muscle						

*Techniques: 120 kVp, 100 mAs, 1 Pitch, 5 mm slice width, 16 x 1.5 mm collimation, and 390 mm scan length*

**Table III** Case record form of thermoluminescent dosimetry for abdominal examination.

“Abdominal examination” Organ	Reading value (mGy)					
	No.1	No.2	No.3	No.4	Average	SD
Gonads						
Bone marrow (red)						
Colon						
Lung						
Stomach						
Bladder						
Breast						
Liver						
Esophagus						
Thyroid						
Skin						
Bone surface						
Kidneys						
Adrenals						
Brain						
Upper large intestine						
Small intestine						
Pancreas						
Spleen						
Thymus						
Uterus						
Muscle						

*Techniques: 120 kVp, 100 mAs, 1 Pitch, 8 mm slice width, 16 x 1.5 mm collimation, and 415 mm scan length*

สถาบันวิทยบริการ  
จุฬาลงกรณ์มหาวิทยาลัย

## APENDIX B

### REPORT OF COMPUTED TOMOGRAPHY SYSTEM PERFORMANCE

**LOCATION:** CT room, Chullajakrapong Building

**DATE:** 5 March, 07

**MANUFACTURER:** Siemens Sensation 16

Procedure of CT system performance:

1. Alignment of table to gantry
2. Table increments accuracy
3. Scan localization light accuracy
4. Slice thickness accuracy
5. Slice increment accuracy
6. Gantry tilt
7. Position dependence and S/N ratio of CT numbers
8. Reproducibility of CT numbers
9. Linearity of CT numbers
10. High contrast resolution
11. Low contrast resolution
12. mAs linearity
13. Multiple scan average dose

สถาบันวิทยบริการ  
จุฬาลงกรณ์มหาวิทยาลัย

## 1. Alignment of table to gantry

**Purpose:** To ensure that long axis of the table is horizontally aligned with a vertical line passing through the rotational axis of the scanner.

**Method:** Locate the table midline using a ruler and mark it on a tape affixed to the table. With the gantry untilted, extend the table top into gantry to tape position. Measure the horizontal deviation between the gantry aperture centre and the table midline. The deviation should be within 5 mm.

**Table IV** Results of alignment of table to gantry.

	Table (mm)	Bore (mm)
Distance from right to center	210.00	349.50
Distance from center to left	197.50	339.00
Measured deviation	6.25	5.25
<i>Measured deviation = (Distance from right to center - Distance from center to left) / 2</i>		

Comment: Results of alignment of table to gantry were not pass.

## 2. Table increments accuracy

**Purpose:** To determine accuracy and reproducibility of table longitudinal motion.

**Method:** Tape a measuring tape at the foot end of the table. Place a paper clip at the center of the tape to function as an indicator. Load the table uniformly with 150 lbs. From the initial position move the table 300, 400 and 500 mm into the gantry under software control (inlet). Record the relative displacement of the pointer on the ruler. Reverse the direction of motion (outlet) and repeat. Repeat the measurements four times. Positional errors should be less than 3 mm at 300 mm position.

**Table V** Result of table increments accuracy.

Indicated (mm)	Measured (mm)	Error (mm)
300	300.5	0.5
400	400.5	0.5
500	500.5	0.5
- 300	- 299.5	0.5
- 400	- 399.5	0.5
- 500	- 499.5	0.5
<i>Error =   Indicated – Measured  </i>		

### 3. Scan localization light accuracy

**Purpose:** To test congruency of scan localization light and scan plane.

**Method:** Tape localization film to the backing plate making sure that the edges of the film are parallel to the plate edge. Place the film vertically along the midline of the couch aligned with its longitudinal axis. Raise the table to the head position. Turn the alignment light. Mark both internal and external light with unique pin pricks along the midline of the light. Expose the internal light localization using the narrowest slice setting at 120-140 kVp, 50-100 mAs, for external light increment table to light position under software control and expose the film. The center of the irradiation field from the pin pricks should be less than 2 mm.

**Results:**

Measured deviation = 0 mm

Internal = 0 mm

External = 0 mm

### 4. Slice thickness accuracy

**Purpose:** To determine the accuracy of the slice thickness.

**Method:** Set up as you would for beam profile measurement. Select 120 kVp, 100 mAs, smallest slit width. Perform several scans with different programmed slice thicknesses under auto control. Scan the film with a densitometer and measure the full width at half maximum distance.

**Table VI** Results of slice thickness accuracy.

Slice thickness (mm)	Measured (mm)	Error (mm)
3.0	3.7	0.7
4.5	5.5	1.0
9.0	10.5	1.5
10.0	12.0	2.0

*Error = | Slice thickness – Measured |*

## 5. Slice increment accuracy

**Purpose:** To determine the accuracy of the slice increment.

**Method:** Set up as you would for beam profile measurement. Select 120 kVp, 100 mAs, smallest slit width. Perform several scans with different programmed slice separations under auto control. Scan the film with a densitometer and measure the distance between the peaks.

**Table VII** Results of slice increment accuracy.

Slice separation (mm)	Measured separation (mm)	Error (mm)
20	21.0	1.0
30	30.5	0.5
50	51.5	1.5

*Error = | Slice separation – Measured separation |*

## 6. Gantry tilt

**Purpose:** To determine the limit of gantry tilt and the accuracy of tilt angle indicator.

**Method:** Tape a localization film to the backing plate making sure that the edges of the film are parallel to the edges of the backing plate. Place the film vertically along the midline of the couch aligned with its longitudinal axis. Raise the table to the head position. Move the table into the gantry, center plate to alignment light. Expose the film at inner light location using narrowest slit, 120-140 kVp, 50-100 mAs. Tilt the gantry to one extreme from the console. Record the indicated gantry angle. Expose the film using the above technique. Measure the clearance from the closest point of gantry to midline of the table. Tilt the gantry to its extreme in the opposite direction. Record clearance and repeat the exposure. Measure the tilt angles from the images on the film. Deviation between indicated and measured tilt angles  $\leq 3^\circ$ . Gantry clearance should be  $\geq 30$  cm.

**Table VIII** Results of gantry tilt and gantry clearance.

	Away	Towards
Indicated angle (degree)	+ 26.5	- 26.5
Measured angle (degree)	+ 26.5	- 26.0
Error (degree)	0	0.5
Clearance (cm)	34.6	36.2

*Error = | Indicated angle – Measured angle |*

## 7. Position dependence and S/N ratio of CT numbers

**Method:** Position the CATPHAN phantom centered in the gantry. Using 1 cm slice thickness, obtain one scan using typical head technique. Select a circular region of interest of approximately 400 mm<sup>2</sup>. And record the mean CT number and standard deviation for each of the positions 1 through 5.

**Technique:** 120 kVp, 320 mA, 1s, 230 mm FOV, and 10 mm slice thickness

**Table IX** Results of position dependence and S/N ratio of CT numbers.

Position	Mean CT number	Standard deviation	CV
1 (12 o' clock)	5.4	2.6	0.48
2 (3 o' clock)	4.9	2.7	0.55
3 (6 o' clock)	5.4	2.6	0.48
4 (9 o' clock)	4.7	2.6	0.55
5 (center)	7.7	3.0	0.39

*CV = Standard deviation / Mean CT number*

## 8. Reproducibility of CT numbers

**Method:** Using the same set up and technique as position dependence, obtain three scans. Using the same ROI as position dependence in location 5, which is the center of the phantom, obtain mean CT numbers for each of the four scans. The coefficient of variation of mean CT numbers of the four scans should be less than 0.002.

**Table X** Results of reproducibility of CT numbers.

Run number	1	2	3	4	Average	SD
CT number	7.7	7.7	7.7	7.7	7.7	0
CV = 0						



## 9. Linearity of CT numbers

**Method:** Set up the mini CT performance phantom as described in beam alignment. Select the section containing the test objects of different CT numbers. Select the head technique and perform a single transverse scan. Select a region of interest (ROI) of sufficient size to cover the test objects. Place the ROI in the middle of each test object and record the mean CT number.

**Technique:** 120 kVp, 250 mA, 1 s, 230 mm FOV, and 10 mm slice thickness

**Table XI** Results of linearity of CT numbers measured by CATPHAN phantom.

Material	$\mu$ ( $\text{cm}^{-1}$ )	Nominal CT number (HU)	CT number (HU)	Deviation from nominal
Air	0.000	- 1000	- 1020.8	20.8
PMP	0.227	- 200	- 199.2	0.8
LDPE	0.174	- 100	- 108.1	8.1
Polystyrene	0.171	- 35	- 47.5	12.5
Acrylic	0.215	120	120.8	0.8
Delrin <sup>TM</sup>	0.245	340	494.1	154.1
Teflon	0.363	990	1394.2	404.2

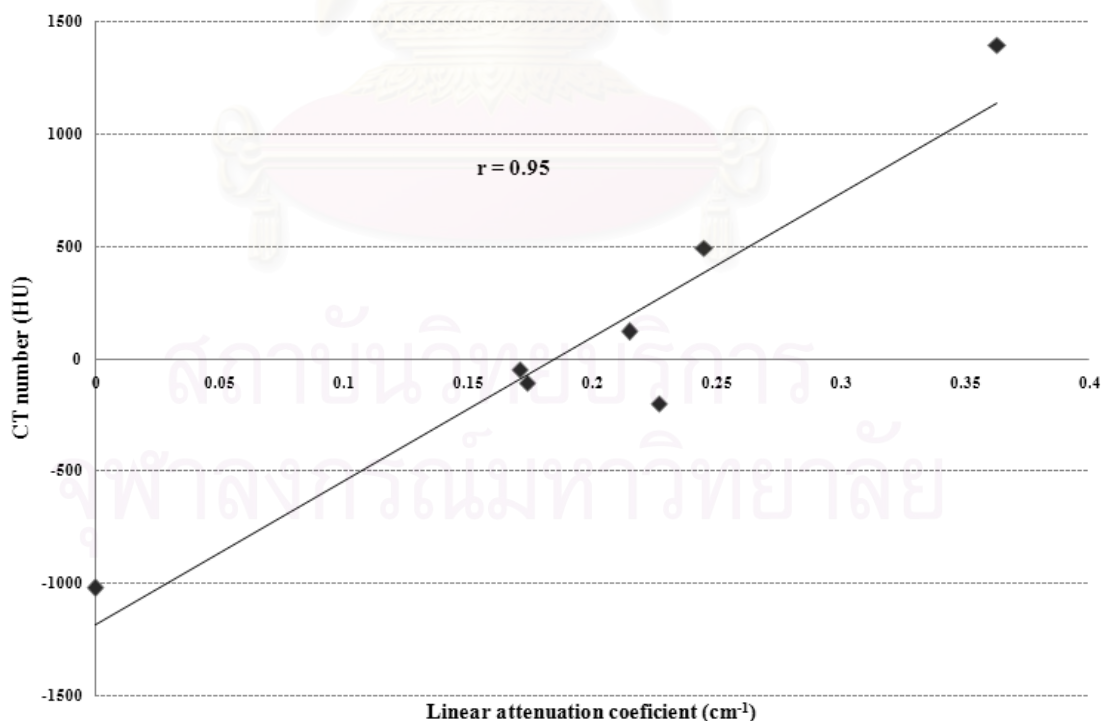


**Figure I** Linearity of CT number.

## 10. High contrast resolution

**Method:** Set up the mini CT performance phantom as described in beam alignment. Select the section containing the high resolution test objects. Select the head technique. Perform a single transverse scan. Select the area containing the high resolution test objects and zoom as necessary. Select appropriate window and level for the best visualization of the test objects. Record the smallest test object visualized on the film.

**Technique:** 120 kVp, 250 mA, 1 s, 230 mm FOV, and 10 mm slice thickness  
Window width = 150, window level = 200

**Table XII** Results of high contrast resolution measured by CATPHAN phantom.

Slice thickness (mm)	Resolution (lp/cm)
10.00	6
5.00	7
3.00	7
0.75	7

## 11. Low contrast resolution

**Method:** Select the section containing the low resolution test objects in the mini phantom. Perform a single transverse scan utilizing the same technique as high resolution.

**Technique:** 120 kVp, 250 mA, 1 s, 230 mm FOV, and 10 mm slice thickness  
Window width = 140, window level = 100

**Table XIII** Results of low contrast resolution (minimum resolvable diameter [mm]) detected by CATPHAN phantom.

	1 % mm	0.5% mm	0.3% mm
Supra-slice	3	4	9
Sub slice 7 mm	5		
Sub slice 5 mm	7		
Sub slice 3 mm	9		

## 12. mAs linearity

**Method:** Set up the same as position dependence and insert 10 cm long pencil chamber in the center slot of the CT dose head phantom. Select the same kVp and time as used for head scan. Obtain four scans in each of the mA stations normally used in the clinic. For each mA station record the exposure in R for each scan. Scans should be performed in the increasing order of mA. Compute R/mAs for each mA setting.

**Technique:** 120 kVp, 1 s, 230 mm FOV, and 10 mm slice thickness

**Table XIV** Results of mAs linearity.

mA	Exposure (R)				Average (R)	R/mAs
	No.1	No.2	No.3	No.4		
150	2.26	2.27	2.26	2.27	2.27	0.02
200	3.03	3.03	3.03	3.03	3.03	0.02
250	3.79	3.79	3.79	3.80	3.79	0.02
320	4.86	4.85	4.85	4.86	4.86	0.02

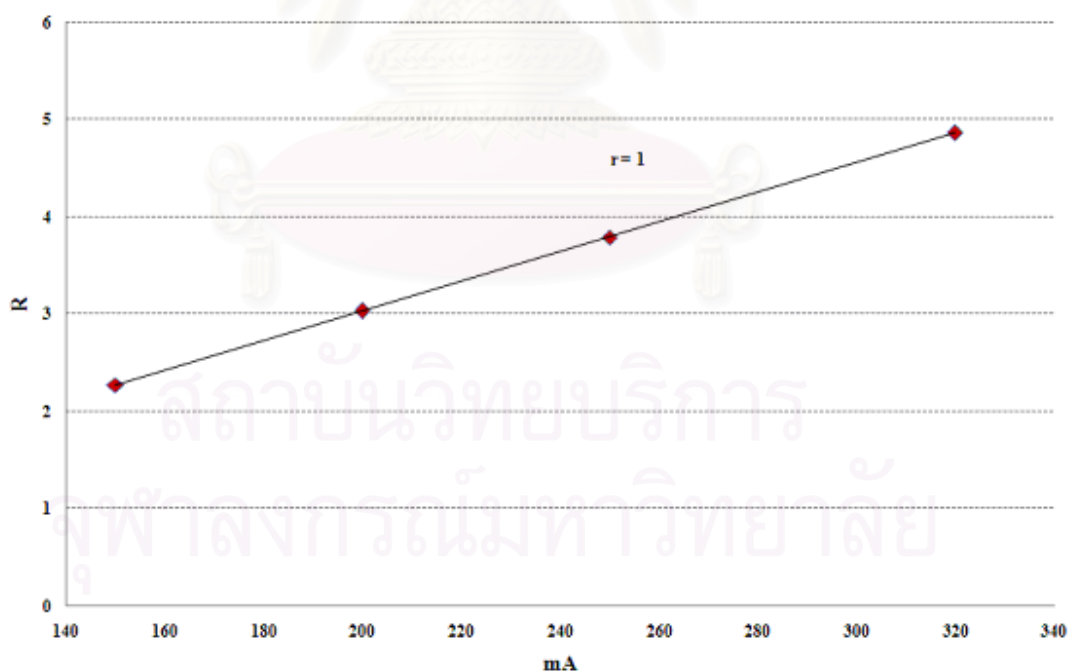


**Figure II** Correlation of R and mA.

### 13. Multiple scan average dose

<b>Skull technique</b>		<b>Exposure in mR</b>	
<b>kVp</b>	120	<b>Run Number</b> 1	4.86
<b>mA</b>	320	2	4.85
<b>Scan time</b>	1 s	3	4.85
<b>Slice thickness</b>	10 mm	4	4.86
<b>Slice Increment</b>	0	<b>Mean Exposure</b>	4.86
<b>Mean Exposure</b>	4.86		
<b>SD</b>	0.01		
<b>CV</b>	0.002		
<b>Calculated MSAD</b>	0.004	<b>rad</b>	

**Figure III** Calculated of multiple scan average doses.

$$MSAD = (E \times f \times K \times L) / T$$

E = Average exposure reading

f = Factor to convert exposure in air to absorbed dose = 0.00078 rad/mR

K = Calibration factor of radiation measuring system = 1

L = Effective length (mm) of radiation measuring system

T = Tomographic slice thickness in mm

สถาบันวิทยบริการ  
จุฬาลงกรณ์มหาวิทยาลัย

## APENDIX C

### UNCERTAINTY OF TLD MEASUREMENT

**Table XV** Uncertainty budgets and the expanded uncertainty of dose measurement using TLD measurement in Rando phantom.

Sources of uncertainty	SD	n	Value* (%)	Probability distribution	Divisor	Uncertainty (%)
1. TLD sensitivity	5.28	1	5.28	Normal	1	5.28
2. TLD calibration						
- TLDs	2.00	3	1.15	Normal	1	1.15
- Ionization chamber repeatability	0.29	3	0.17	Normal	1	0.17
3. Calibration factor of ionization chamber (calibration certificate)	0.60	1	0.60	Normal	2	0.30
4. Measuring accuracy	3.17	3	1.83	Normal	1	1.83
Combined uncertainty						<b>5.72</b>
Expanded uncertainty (k=2), 95% confidence level						<b>11.74</b>

\*Standard uncertainty

#### Steps of determination the values of uncertainty budgets

**Step 1:** Calculated value of standard uncertainty

1. TLD sensitivity (nC)

The estimated standard deviation = 5.28

$$\text{Standard uncertainty for the type A from 1 reading} = \frac{SD}{\sqrt{n}} = \frac{5.28}{\sqrt{1}} = 5.28\%$$

2. TLD calibration

2.1 TLDs (nC)

The mean value = 285

The estimated standard deviation = 2.00

$$\text{Standard uncertainty for the type A from 3 readings} = \frac{SD}{\sqrt{n}} = \frac{2}{\sqrt{3}} = 1.15\%$$

2.2 Ionization chamber repeatability (mGy)

The mean value = 5.95

The estimated standard deviation = 0.29

$$\text{Standard uncertainty for the type A from 3 readings} = \frac{SD}{\sqrt{n}} = \frac{0.29}{\sqrt{3}} = 0.17\%$$

### 3. Calibration factor of ionization chamber (calibration certificate)

The estimated standard deviation = 0.60

$$\text{Standard uncertainty for the type A from 1 reading} = \frac{SD}{\sqrt{n}} = \frac{0.6}{\sqrt{1}} = 0.60\%$$

### 4. Measuring accuracy (nC)

The mean value = 301.07

The estimated standard deviation = 3.17

$$\text{Standard uncertainty for the type A from 3 readings} = \frac{SD}{\sqrt{n}} = \frac{3.17}{\sqrt{3}} = 1.83\%$$

### Step 2: Calculated uncertainty

$$1. \text{ Uncertainty} = \frac{\text{Value}}{\text{Divisor}} = \frac{5.28}{1} = 5.28\%$$

$$2.1 \text{ Uncertainty} = \frac{\text{Value}}{\text{Divisor}} = \frac{1.15}{1} = 1.15\%$$

$$2.2 \text{ Uncertainty} = \frac{\text{Value}}{\text{Divisor}} = \frac{0.17}{1} = 0.17\%$$

$$3. \text{ Uncertainty} = \frac{\text{Value}}{\text{Divisor}} = \frac{0.6}{2} = 0.30\%$$

$$4. \text{ Uncertainty} = \frac{\text{Value}}{\text{Divisor}} = \frac{1.83}{1} = 1.83\%$$

### Step 3: Calculated combined uncertainty

$$\text{Combined uncertainty} = \sqrt{5.28^2 + 1.15^2 + 0.17^2 + 0.3^2 + 1.83^2} = 5.72\%$$

### Step 4: Calculated expanded uncertainty

$$\text{Expanded uncertainty (k=2)} = \text{Combined uncertainty} \times 2 = 5.72 \times 2 = 11.74\%$$

**VITAE**

**NAME** Boonserm Nerysungnoen

**SEX** Male

**NATIONALITY** Thai

**DATE OF BIRTH** November 19, 1972

**PLACE OF BIRTH** Nakhon Ratchasima, Thailand

**INSTITUTIONS ATTENDED** Khonkaen University, 2005:  
Bachelor of Science  
(Radiological Technology)

Chulalongkorn University, 2008:  
Master of Science  
(Medical Imaging)

**HOME ADDRESS** 71 Moo 2, T.Nongtakai, A.Sungnoen,  
Nakhon Ratchasima 30380

**POSITION HELD & OFFICE** 1994 to present  
Department of Radiology  
Maharat Nakhon Ratchasima Hospital,  
Nakhon Ratchasima, Thailand  
Position: Radiological Technologist

สถาบันวิทยบริการ  
จุฬาลงกรณ์มหาวิทยาลัย